

AD-A136045

"
RESEARCH ON NEW APPROACHES TO OPTICAL
SYSTEMS FOR INERTIAL ROTATION SENSING"
"

FINAL REPORT

for

Grant No. AFOSR F49620-82-K-0029

Prepared for

Air Force Office of Scientific Research
Bolling Air Force Base
Washington, D. C. 20332

for the period

1 May 1982 - 30 June 1983

G. L. Report No. 3622

DTIC
ELECTE
DEC 20 1983
S B D

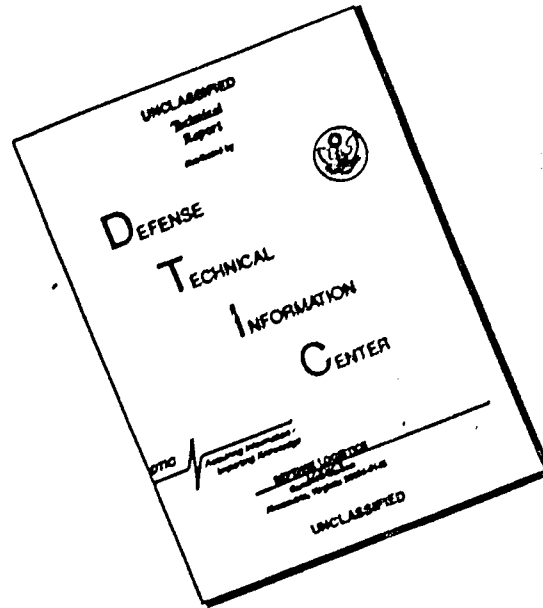
DTIC FILE COPY

Edward L. Ginzton Laboratory
W. W. Hansen Laboratories of Physics
Stanford University
Stanford, California 94305

Approved for public release;
distribution unlimited.

The views and conclusions contained in this document are those of the authors and should not be interpreted as necessarily representing the official policies or endorsements, either expressed or implied of the Air Force Office of Scientific Research or the U.S. Government.

DISCLAIMER NOTICE



THIS DOCUMENT IS BEST QUALITY AVAILABLE. THE COPY FURNISHED TO DTIC CONTAINED A SIGNIFICANT NUMBER OF PAGES WHICH DO NOT REPRODUCE LEGIBLY.

REPORT DOCUMENTATION PAGE		READ INSTRUCTIONS BEFORE COMPLETING FORM										
1. REPORT NUMBER AFOSR-TR- 83 - 0884	2. GOVT ACCESSION NO. AD-A136045	3. RECIPIENT'S CATALOG NUMBER										
4. TITLE (and Subtitle) New Approaches to Optical Systems for Inertial Rotation Sensing		5. TYPE OF REPORT & PERIOD COVERED Final Report 1 May 1982 - 30 June 1983										
		6. PERFORMING ORG. REPORT NUMBER G.L. 3622										
7. AUTHOR(s) Multiple authors		8. CONTRACT OR GRANT NUMBER(s) F49620-82-K-0029										
9. PERFORMING ORGANIZATION NAME AND ADDRESS Stanford University Edward L. Ginzton Laboratory Stanford, California 94305		10. PROGRAM ELEMENT, PROJECT, TASK AREA & WORK UNIT NUMBERS 2305/B2 6/102F										
11. CONTROLLING OFFICE NAME AND ADDRESS Directorate of Electronic & Material Sciences AFOSR/NE Building 410, Bolling AFB DC 20332		12. REPORT DATE 30 JUN 1983										
		13. NUMBER OF PAGES 77										
14. MONITORING AGENCY NAME & ADDRESS (if different from Controlling Office)		15. SECURITY CLASS. (of this report) Unclassified										
		15a. DECLASSIFICATION/ DOWNGRADING SCHEDULE N/A										
16. DISTRIBUTION STATEMENT (of this Report) Approved for public release; distribution unlimited.												
17. DISTRIBUTION STATEMENT (of the abstract entered in Block 20, if different from Report)												
18. SUPPLEMENTARY NOTES												
19. KEY WORDS (Continue on reverse side if necessary and identify by block number)												
<table border="0"> <tr> <td>Inertial Rotation Sensing</td> <td>Optical Fiber Amplifier</td> </tr> <tr> <td>Optical Sagnac Interferometer</td> <td>Nd:YAG Fiber Amplifier</td> </tr> <tr> <td>Passive Re-entrant Fiber Gyro</td> <td>Spherical Aberration, Lens Aberration</td> </tr> <tr> <td>Bidirectional Optical Amplifiers</td> <td>Source Coherence</td> </tr> <tr> <td>(Bilateral Optical Amplifier)</td> <td>Phase Noise</td> </tr> </table>			Inertial Rotation Sensing	Optical Fiber Amplifier	Optical Sagnac Interferometer	Nd:YAG Fiber Amplifier	Passive Re-entrant Fiber Gyro	Spherical Aberration, Lens Aberration	Bidirectional Optical Amplifiers	Source Coherence	(Bilateral Optical Amplifier)	Phase Noise
Inertial Rotation Sensing	Optical Fiber Amplifier											
Optical Sagnac Interferometer	Nd:YAG Fiber Amplifier											
Passive Re-entrant Fiber Gyro	Spherical Aberration, Lens Aberration											
Bidirectional Optical Amplifiers	Source Coherence											
(Bilateral Optical Amplifier)	Phase Noise											
20. ABSTRACT (Continue on reverse side if necessary and identify by block number)												
<p>This report describes further progress in the development of fiber optic Sagnac loops for inertial rotation sensing (i.e., fiber gyros). The report consists mainly of two sections. The first section describes work on developing a bi-directional optical amplifier for use in fiber optic sensing loops while the second section deals with limits on rotation sensitivity due to fiber scattering and noise statistics of optical sources.</p> <p>The sensitivity of the existing passive re-entrant Sagnac system (described in</p>												

19.

Laser Spectra
 Rayleigh Backscattering
 Correlated Backscattering
 Uncorrelated Backscattering
 Intensity Saturation

Single Mode Fiber
 All Fiber Gyro
 Laser Noise
 Laser Fluctuation

20.

in a previous report) can be enhanced if the signal attenuation in the sensing loop can be minimized. This can be accomplished by the addition of an optical amplifier to compensate for the loop losses. Three distinct approaches are analyzed theoretically with expressions derived to predict the expected signal gains. Experimental results on two of the approaches are included which demonstrate some of the problems and advantages associated with each. Also included in the section on optical amplifiers is a theoretical analysis of coupling efficiencies into single mode fibers after Gaussian beams are focused by using spherical lenses. This is important since the above amplifier schemes involve lenses which operate on the signal beam as it travels through the amplifier.

In the final section of the report the minimum measurable rotation rate in fiber optic systems due to either noise from the optical source or backscattering in fiber sensing loops is investigated. Phase and amplitude noise found in existing optical sources are discussed with recommendations given on types of sources best suited for fiber gyro applications. The effect of both correlated and uncorrelated optical backscattering in optical fiber gyros is analyzed theoretically to provide expressions relating minimum measurable rotation rates in the presence of these effects. Representative values for scattering parameters are used to obtain quantitative results for comparison with other sources of error.

Accession For	
NTIS GRA&I	<input checked="" type="checkbox"/>
DTIC TAB	<input type="checkbox"/>
Unannounced	<input type="checkbox"/>
Justification	
By _____	
Distribution/	
Availability Codes	
Dist	Avail and/or Special
A-1	



UNCLASSIFIED

TABLE OF CONTENTS

I.	INTRODUCTION	1
II.	OPTICAL AMPLIFIERS FOR THE RE-ENTRANT FIBER GYRO	3
	A. Optical Amplifier	3
	1. Introduction	3
	2. Theory	4
	a. Fiber-Slab Amplifier	8
	b. Single Rod Amplifier	12
	c. Index Guided Amplifier	15
	3. Experimental Results	17
	4. Conclusion	28
	B. Spherical Aberration From Single Element Lenses	28
	1. Introduction	28
	2. Theory	29
	3. Results	31
	4. Conclusion	42
III.	SOURCE NOISE AND SCATTER LIMITATIONS	43
	A. Introduction	43
	B. The Effect of Signal Statistics on Optical Fiber Gyros	44
	1. Some Basic Concepts, Coherence	44
	2. Fluctuation in the Primary Signal	46
	C. The Effect of Scattering on Optical Fiber Gyros	51
	1. Fluctuation and Error Due to Backscatter	51
	2. Correlated Components	57
	3. Uncorrelated Components	60
	4. Scatter Equivalent Phase and Rotation Error	62
IV.	APPENDIX	

AIR FORCE OFFICE OF SCIENTIFIC RESEARCH (AFSC)
 NOTICE OF TRANSMITTAL TO DTIC
 This technical report has been reviewed and is
 approved for public release IAW AFR 190-12.
 Distribution is unlimited.
 MATTHEW J. KERPER
 Chief, Technical Information Division

A.	Sensitivity of Sagnac, Using An AC Bias	65
B.	AC Bias Modulation of the Correlated Scatter	68
C.	Shot Noise Output	69
V.	BIBLIOGRAPHY	71

I. INTRODUCTION

This report covers research under Grant F49620-82-K-0029 for the period from May 1, 1982 through June 30, 1983. Work done during the period from May 1, 1981 through April 30, 1982 is covered in an earlier report.

The objective of this research program has been to investigate the characteristics of new fiber optic configurations for inertial rotation sensing with the aim of extending the sensitivity threshold and basic stability of such systems, and to extend the range of operation to very fast as well as very slow rates. The program has involved basic device research, including both theoretical analyses and experimental demonstrations of specific configurations. It also has included research on novel component devices for use in these systems.

The principal experimental approach to rotation sensing which has been studied up to now has been referred to as a Passive Re-entrant Sagnac System (PRS). Like the more conventional fiber gyro, it uses a multiturn optical fiber sensing coil, but it recirculates pulses of light, and successive readings of the phase shift provide an integrated phase shift due to rotation. This results in a direct measure of angular rotation rather than a measure of rotation rate. Operation and demonstration of such an all fiber re-entrant Sagnac system was reported in detail in the previous contract report.

Re-entrant Sagnac systems differ from the more common optical fiber rotation sensors in that a pulsed optical signal is first split and then introduced in opposite directions into the loop of fiber. The interference of the counterpropagating pulses is monitored as the pulses recirculate many times. In a rotating system the cumulative phase difference between the two recirculating pulses results in a sinusoidally modulated pulse train that is a direct measure of the angle through which the system has turned. This is an advantage over more conventional fiber gyros that produce a signal proportional to the rate of rotation which then must be electroni-

cally integrated.

The sensitivity of the passive re-entrant Sagnac system depends upon the length of time that the recirculating light pulses can be continuously monitored before they are lost in the noise. At present, this time is limited by the attenuation in the fiber along with the losses in coupling the light into and out of the fiber loop. To overcome this limitation a bi-directional optical amplifier is needed for insertion into the fiber loop. The loop losses can then be compensated for by use of the amplifier so that the recirculating light pulses experience no net attenuation. The needed optical amplifier should preserve the single mode nature of the signal and be compatible with single mode fiber. It will need to provide several dB of gain to compensate for the present losses in the fiber loop. Since an optical amplifier must be pumped in some manner (to produce a population inversion in the active medium) it is important that this pumping scheme be efficient so as not to require too large a pump source. A major portion of the reporting period has been focussed on the components and on the understanding necessary for refinement of the passive re-entrant gyro so as to include active elements, making what we call an Active Re-entrant Sagnac System (ARS). The goal of the research is to achieve sensitivities equal to, and in some cases larger than, with other laser gyro systems, and with advantages in overcoming drift error, and with the ability to measure high rates of rotation without ambiguity.

The ultimate sensitivity of any fiber loop gyro cannot exceed that allowed for by the signal source or material that guides it. A portion of this report addresses the questions of fiber backscattering and signal source statistics. These questions are important in determining the maximum sensitivity possible in optical fiber gyros. This work is not restricted to re-entrant type fiber gyros, but is applicable to fiber gyros in general.

The following report consists of two major sections. The first section deals

with the development of an optical amplifier for insertion into the existing passive re-entrant gyro. Theoretical analysis is carried out on three different amplifier approaches with expressions derived to predict the expected gains. Experimental measurements are included on two of these amplifier approaches which point out advantages and disadvantages of the specific configuration employed. Also included in the amplifier section is theoretical investigation of mode distortion as the signal is transferred through spherical lenses. The present amplifier schemes include the use of lenses in focussing the signal through the gain medium and back into the single mode fiber. Since the losses generated in the focussing process must be compensated for by extra gain through the amplifier it is important to understand quantitatively the efficiencies that can be expected from the focussing elements.

The second section of the report theoretically investigates how statistical variations in the optical source and scattering in the fiber effect the measured output obtained from fiber gyros. The coherence and amplitude stability of existing optical sources is discussed showing how these statistical variations can effect the output signal. Also included in the output signal is the effect of correlated and uncorrelated scattering components due to the inherent scattering processes found in all optical fibers. Representative numerical values are then used to show the quantitative effects of these error mechanisms.

II. OPTICAL AMPLIFIERS FOR RE-ENTRANT FIBER GYRO

A. Optical Amplifiers

1. Introduction

Optical amplifiers designed for compatibility with single mode optical fibers are needed to enhance the performance of many fiber devices now being developed.

These optical amplifiers would require net gains of 2 or 3 dB to overcome the losses due to optical components and fiber attenuation in recirculating pulsed systems. Direct optical amplification as opposed to electrical repeater type schemes offer much larger bandwidths and the preservation of phase information which is needed for the short pulses and interferometric techniques used in many fiber systems.

Optical amplifiers would be used to enhance fiber signal processing systems, increase the storage time in fiber optic memories, convert the fiber resonator into a ring fiber laser and increase the rotation sensitivity of re-entrant pulsed fiber gyros. to mention only a few of its many applications.

2. Theory

The approach we have initially taken is to use a laser beam to optically pump a gain medium such as a Nd:YAG crystal. For efficient amplification both the pump and signal beams should travel collinearly through the gain medium (see Fig. II-1). A combination of high pump and signal intensities together with long interaction lengths will result in the maximum gain for a given pump power. An optimum arrangement that satisfies the above conditions would be to make an amplifier out of a section of single mode fiber whose core region contains an active gain medium. Because of the development time and expense associated with such an amplifier it was decided to focus initial efforts on the design of an amplifier using a nonguiding gain medium. This should result in the development of a useable amplifier in the minimum amount of time.

In a four-level gain medium the steady-state population inversion density (atoms/cm³) due to a non-saturating pump intensity $I_p(x, y, z)$ is given by

$$n_2(x, y, z) = \frac{\alpha_p \tau_2}{h\nu_p} \cdot \eta_0 \cdot I_p(x, y, z) \quad (II-1)$$

where α_p is the exponential absorption coefficient of the pump radiation, τ_2 is the

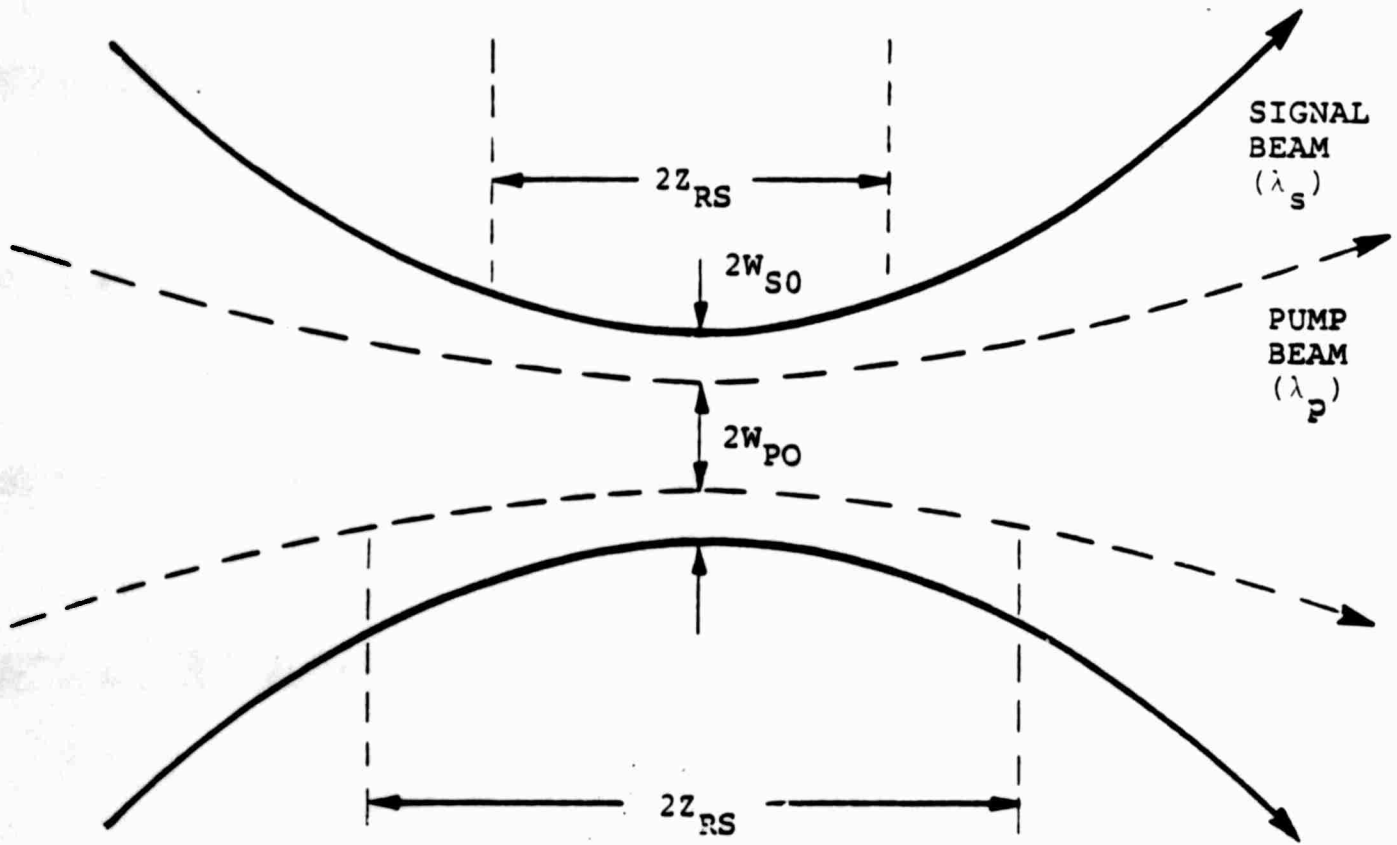


Fig. II-1. Side view of pump and signal beams in unguided gain medium.

average inversion lifetime of an atom, $h\nu_p$ is the energy of a pump photon and η_0 is the quantum efficiency for producing a radiated photon for each pump photon absorbed. Equation II-1 shows that the population inversion density is proportional to the pump intensity.

The rate of stimulated atoms per volume element (dn_s/dt) for a given signal intensity $I_s(x, y, z)$ can be written as

$$\frac{dn_s(x, y, z)}{dt} = \frac{\sigma_s}{h\nu_s} \cdot n_2(x, y, z) \cdot I_s(x, y, z) \quad (II-2)$$

where σ_s is the stimulated cross-section for an inverted atom and $h\nu_s$ is the stimulated photon energy.

Assuming that all the stimulated atoms contribute in amplifying the signal beam the growth of the signal power per length dP_s/dz is obtained by integrating over all the stimulated atoms.

$$\frac{dP_s}{dz} = h\nu_s \int \int \frac{dn_s}{dt} dx dy \quad (II-3)$$

Combining Eq. (II-1), (II-2) and (II-3) gives

$$\frac{dP_s}{dz} = \frac{\sigma_s \alpha_p \tau_2}{h\nu_p} \eta_0 \int \int I_p(x, y, z) \cdot I_s(x, y, z) dx dy \quad (II-4)$$

Equation II-4 shows that to get the largest growth in signal power per incremental length of gain medium one would like the pump and signal intensities to be as large as possible (assuming we do not reach the regime of pump or signal saturation). For a given pump and signal power the intensities can be made large by focusing the beams to a small area. Although focusing increases the beam intensities to make dP_s/dz large, diffraction in a non-guiding gain medium will cause the beams to diverge more quickly which will limit the effective length over which the signal beam is amplified. This effect is identical to that which limits nonlinear processes

when a pump beam is focused into a bulk crystal. This trade-off between increased intensity but shortened interaction length when using bulk gain mediums is not present when the signal and pump are index guided in the gain medium such as in the case of a single mode fiber with an active core region.

Equation (II-4) can be further simplified if we make some assumptions on spatial structure of the pump and signal intensities. To within a few percent the signal traveling in a single mode fiber can be represented as a lowest order TEM_{00} Gaussian mode. Assuming Gaussian modes in the bulk gain medium we can write the pump and signal intensities as

$$I_p(r, z) = \frac{P_p e^{-\alpha_p z}}{\frac{\pi}{2} W_p^2(z)} e^{-\frac{2r^2}{W_p^2(z)}} \quad (II-5)$$

$$I_s(r, z) = \frac{P_s(z)}{\frac{\pi}{2} W_s^2(z)} e^{-\frac{2r^2}{W_s^2(z)}} \quad (II-6)$$

In Eq. (II-5) the term $P_p e^{-\alpha_p z}$ is due to the absorption of the pump beam as it travels through the gain medium. P_p is the power in the pump beam at the location $z = 0$. $P_s(z)$ in Eq. (II-6) is the power in the signal beam whose form of growth we have left unspecified for now. The beam radii are given by

$$W_p(z) = W_{p0} \sqrt{1 + (z/z_{Rp})^2} \quad (II-7)$$

$$W_s(z) = W_{s0} \sqrt{1 + (z/z_{Rs})^2} \quad (II-8)$$

where z_{Rp} and z_{Rs} are the Rayleigh ranges of the pump and signal beams. W_{p0} and W_{s0} represent the minimum radii of the two beams whose locations are assumed to occur at the same place (see Fig. II-1).

By assuming a Gaussian intensity profile for the cross-section of the pump and signal beams Eq. (II-4) can be integrated to obtain

$$\frac{dP_s}{dz} = \frac{\sigma_s \alpha_p \bar{r}_s^2 \eta_0}{h \nu_p} \cdot \frac{P_p e^{-\alpha_p z}}{\frac{\pi}{2} (W_p^2(z) + W_s^2(z))} \cdot P_s(z) \quad (II-9)$$

medium.

$$P_s(z) = P_{s0} e^{g_0 z} \quad (II - 10)$$

where

$$g_0 = \int \frac{\sigma_s \alpha_p \tau_2 \eta_0}{h \nu_p} \frac{P_p e^{-\alpha_p z}}{\frac{\pi}{2}(W_p^2(z) + W_s^2(z))} dz \quad (II - 11)$$

Considering $\pi/2(W_p^2(z) + W_s^2(z))$ as an effective area of the overlap between the pump and signal beams and $P_p e^{-\alpha_p z}$ as the power in the pump beam we can see that the gain coefficient (g_0) is proportional to an integration over length of an effective pump intensity through the gain medium. A review of the key assumptions made to obtain Eq. (II-11) are:

- (i) All the stimulated photons contribute to the growth of the signal beam.
- (ii) The signal and pump beams are lowest order Gaussian modes whose waists occur at the same location in the gain medium.
- (iii) The pump and signal intensities are small enough to avoid saturation effects in the gain medium.

Although these assumptions may be a bit too restrictive they allow for a relatively simple analytical expression describing the growth of the signal beam which can give some insight into the processes involved in amplifying the signal with a collinear pump.

a. Fiber-Slab Amplifier

The amplifier shown in Fig. II-2 takes advantage of the high intensities of the pump and signal as the two beams leave the small core region of the single mode fiber. Since the gain per unit length falls off quickly as the beams diverge it is advantageous to put a slab of gain medium in contact with the input and output fibers where both the pump and signal intensities are at their maximum. Since the

pump and signal beams have both been combined into a single mode fiber they both share the same optical axis which guarantees good beam overlap and allows for a simple alignment procedure.

Since the most gain will occur near the output of fiber A and the input of fiber B, if we make the slabs too thick all the pump will be absorbed before it gets near fiber B making its contribution to the gain insignificant. If the slabs are too thin the interaction length of the pump and signal beams will be small and this will also cause a decrease in the amplifier gain. This argument shows that there is an optimum thickness for the two slabs which maximizes the gain through the amplifier.

To find this optimum length Eq. (II-11) was numerically integrated to show how the gain coefficient (g_0) varies with the total length of the gain medium. The resulting curve is shown in Fig. II-3. This plot assumes the fibers have a $3 \mu\text{m}$ radius core and the gain medium to be Nd:YAG. It can be seen that the gain coefficient becomes a maximum for a total crystal length of about 1 mm which corresponds to two .5 mm slabs. Figure II-3 also shows that making the slabs too thin can result in a dramatic decrease in gain while too thick of slabs has only a marginal effect. Operating at the optimum Nd:YAG crystal length and pump wavelength of $\lambda_p = 808 \text{ nm}$ ($\alpha_p \simeq 4 \text{ cm}^{-1}$) results in an input pump power of approximately 40 mW to achieve a 3 dB crystal gain. This gain does not include the coupling and reflection losses which would result in a much smaller net gain.

This same analysis was done for a neodymium pentaphosphate ($\text{NdP}_5\text{O}_{14}$) crystal which has a much higher concentration of neodymium atoms. It was found that when using a near optimum pump wavelength of $\lambda_p = 789 \text{ nm}$ ($\alpha_p \simeq 32 \text{ cm}^{-1}$) the max gain occurs for a total crystal length of $\sim .25 \text{ mm}$ (125 μm slabs). Under these conditions a 3 dB crystal gain theoretically requires only 12 mW of pump power.

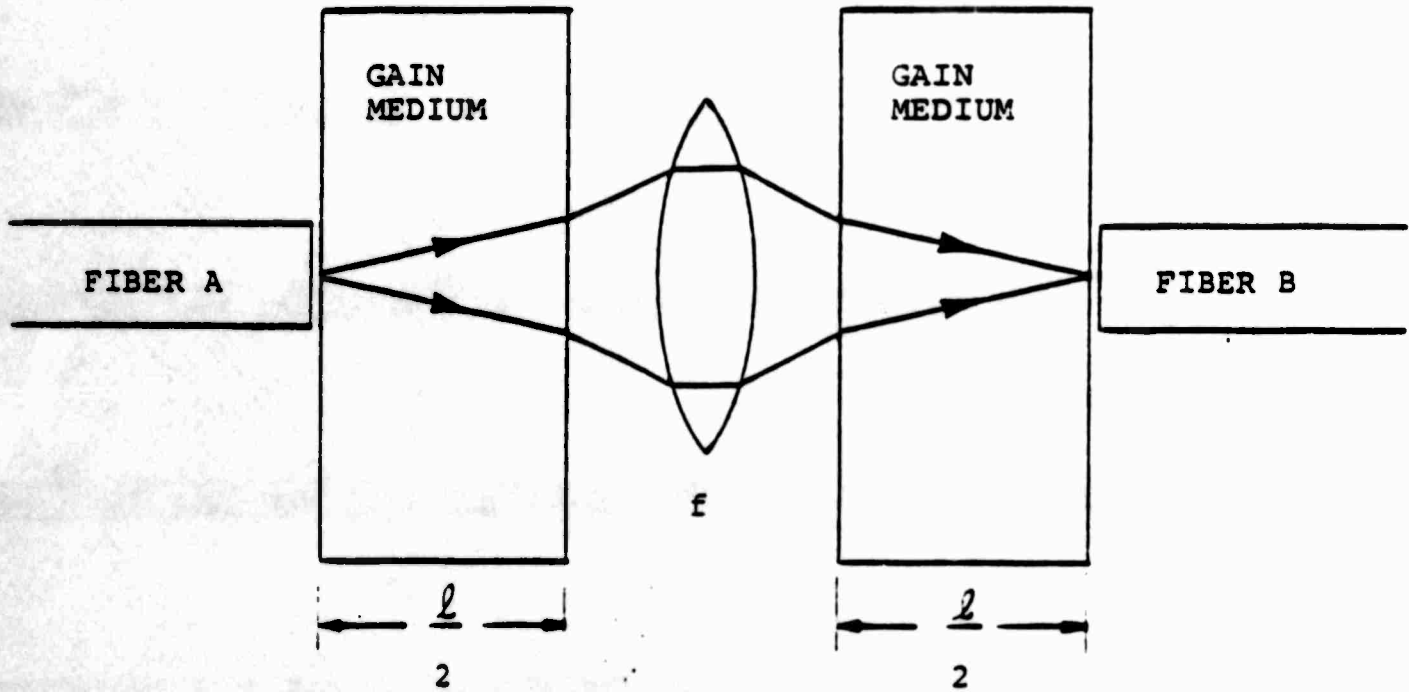
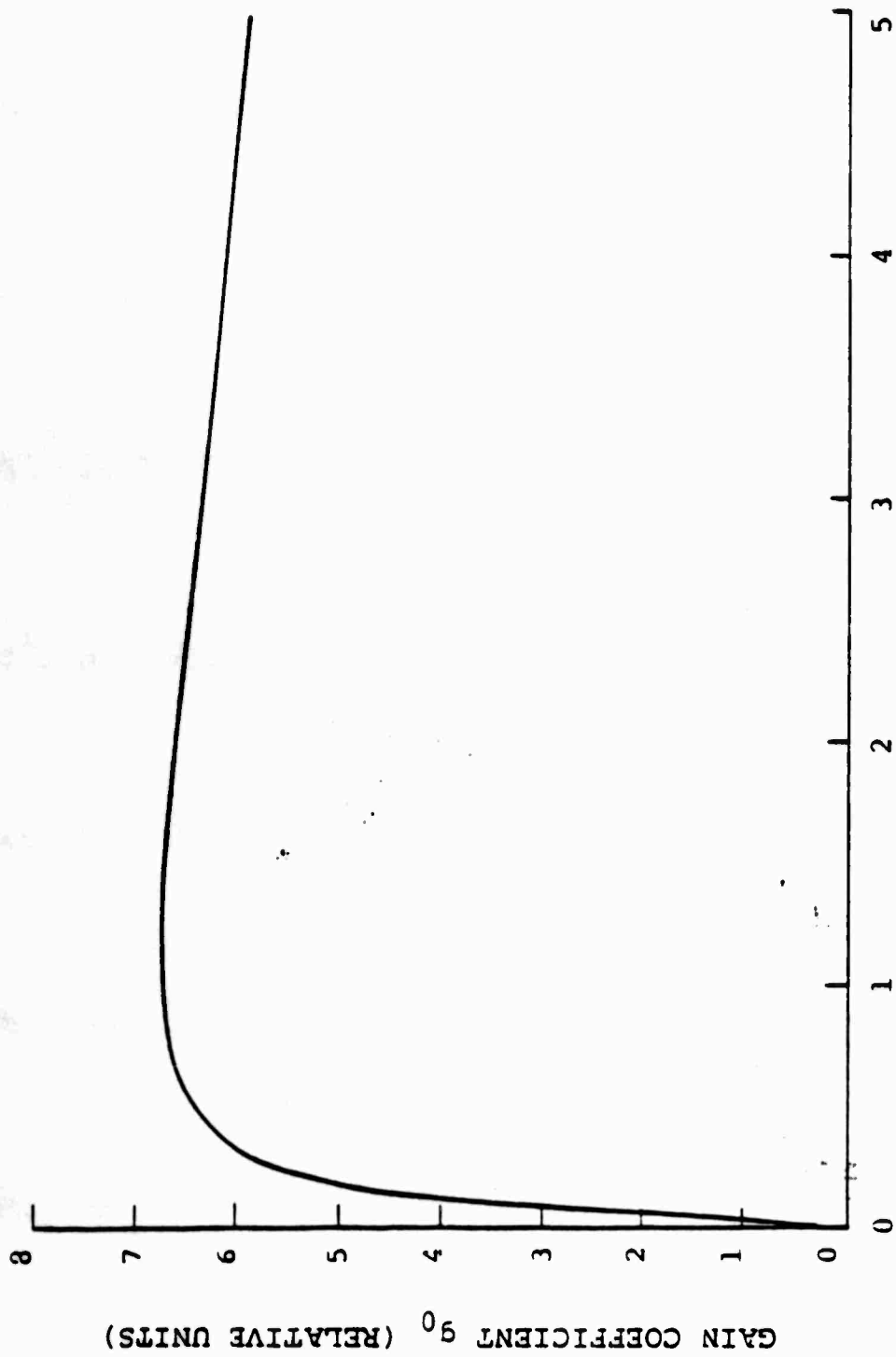


Fig. II-2. Fiber-slab amplifier. Signal and pump beams have been previously combined in Fiber A.



TOTAL CRYSTAL LENGTH l (mm)

Fig. II-3. Gain of fiber-slab amplifier as crystal length varies.
 Crystal = Nd:YAG, $W_{SO} = 3.2 \mu\text{m}$, $W_{PO} = 3.0 \mu\text{m}$, $\alpha_P = 1.1 \text{ cm}^{-1}$.

One of the important assumptions in the calculation of these gains is that the pump beam does not saturate the gain medium. It turns out that the peak intensity of 10 mW and 12 mW in a fiber whose core radius is $3 \mu\text{m}$ is 290 KW/cm^2 and 90 KW/cm^2 respectively. For the two cases considered the saturation pump intensity for Nd:YAG at $\lambda_p = 808 \text{ nm}$ is approximately $I_{sat} \approx 130 \text{ KW/cm}^2$ and for $\text{NdP}_5\text{O}_{14}$ at $\lambda_p = 789 \text{ nm}$ $I_{sat} = 260 \text{ KW/cm}^2$. Since the Nd:YAG example requires a pump intensity above the crystal's saturation intensity the expression for the gain is no longer valid and a 3 dB gain will require more than 40 mW of pump. As for the $\text{NdP}_5\text{O}_{14}$, the pump intensity of 90 KW/cm^2 is quite close to the saturation intensity of 260 KW/cm^2 and the nonsaturated assumption is probably starting to break down. Because of coupling losses between the two fibers a crystal gain of 5 or 6 dB may be required making the needed pump intensities even larger. It would appear that one of the fundamental limitations of the fiber slab amplifier is that of pump saturation which will limit the gain.

b. Single Rod Amplifier

This amplifier scheme is shown in Fig. II-4 where both pump and signal beams are focused into a single rod of gain medium. Because of the ability to focus into the gain medium the beam waists are not constrained to the size of the fiber core like in the previous scheme. This allows for decreasing the pump intensity by enlarging the beam waists, it also has the added benefit that the corresponding Rayleigh ranges also increase which results in longer interaction lengths between the pump and signal.

To avoid numerical integration in calculating the gain coefficient (Eq. (II-11)) we can make an additional assumption by replacing the exponentially decreasing pump power with its value at the midpoint of the crystal (i.e. $P_p e^{-\alpha_p z} \rightarrow P_p e^{-\alpha_p l/2}$ in Eq. (II-11)). This assumption allows Eq. (II-11) to be integrated in closed form

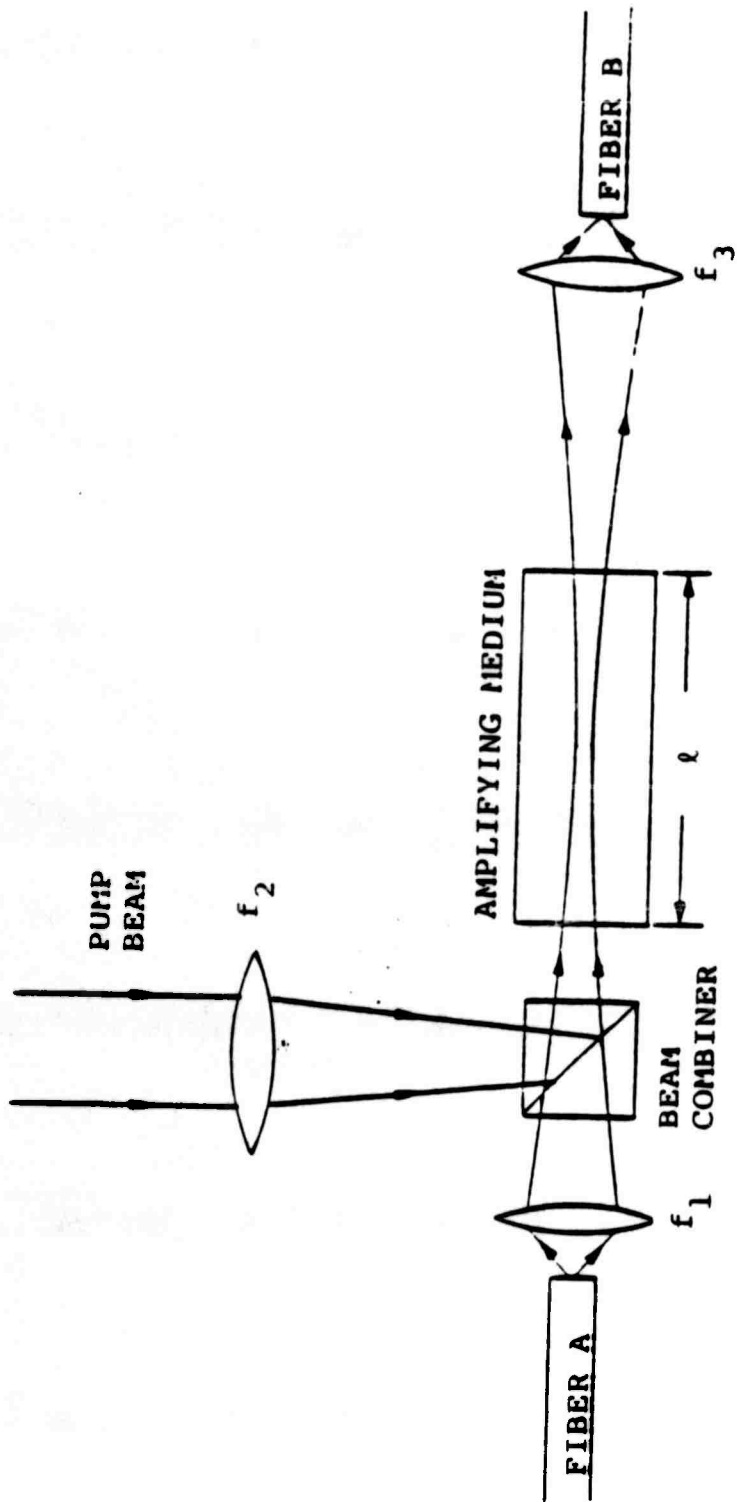


Fig. II-4. Single rod amplifier. Pump beam is combined with signal just before entering amplifying medium.

to give

$$g_0 = \frac{\sigma_s \alpha_p \tau_2 \eta_0}{h \nu_p} \frac{P_p e^{-\alpha_p \ell / 2}}{\pi / 2 (W_{p0}^2 + W_{s0}^2)} 2z_{eff} \tan^{-1} \left(\frac{\ell}{2z_{eff}} \right) \quad (II-12)$$

In Eq. (II-12) z_{eff} is an effective Rayleigh range for the combination of the pump and signal beams whose value is given by

$$z_{eff} = \frac{\pi W_{p0}^2 \eta}{\lambda_p} \sqrt{\frac{1 + \left(\frac{W_{p0}}{W_{s0}} \right)^2}{1 + \left(\frac{\lambda_s W_{p0}}{\lambda_p W_{s0}} \right)^2}} \quad (II-13)$$

In Eq. (II-12) we have assumed that both pump and signal waists occur half way along a crystal rod of length ℓ .

For crystal lengths greater than several Rayleigh ranges and not too long compared to the pump absorption coefficient the crystal gain can be shown to be relatively independent of the crystal length (see Fig. II-3). In this regime the gain coefficient is insensitive to the absolute sizes of the pump and signal waists and depends only on the relative ratio. This effect can be understood by noting that if the beams are focused tighter to increase their intensity, the effective interaction region will be shortened due to stronger beam diffraction. It turns out that the increase in intensity just cancels the effect of the decrease in interaction length which results in a gain coefficient that is insensitive to actual beam sizes. This of course assumes that the beam waists are not made so small as to intensity saturate the gain medium.

It can also be shown that the gain is maximized in Eq. (II-12) when the ratio between pump and signal waists is given by

$$\frac{W_{s0}}{W_{p0}} = \sqrt{\frac{\lambda_s}{\lambda_p}} \quad (II-14)$$

This condition of maximizing the gain also satisfies the condition that both pump and signal Rayleigh ranges are equal which in turn is identical to the effective

Rayleigh range z_{eff} . Since the pump wavelength will always be shorter than the signal wavelength this implies that the waist of the signal should be slightly larger than that of the pump.

After optimizing the gain in Eq. (II-12) for both spot size ratio and crystal length, the required pump powers for a 3 dB gain are calculated for the same two gain materials as used in the fiber-slab amplifier example. For Nd:YAG at $\lambda_p = 808 \text{ nm}$ ($\alpha_p = 4 \text{ cm}^{-1}$) the optimum rod length was calculated to be 1.52 mm. this optimum length was determined by the first picking the pump and signal spot sizes ($W_{p0} = 10 \mu\text{m}$, $W_{s0} = 11.5 \mu\text{m}$) which in turn were picked so that the pump intensity for a 3 dB gain is approximately a order of magnitude below the saturation intensity. Using these optimized parameters a 3 dB crystal gain requires approximately 77 mW.

For the case of $\text{NbP}_5\text{O}_{14}$ with $\lambda = 803 \text{ nm}$ ($\alpha_p = 59 \text{ cm}^{-1}$) the optimum rod length was .167 mm for spot sizes of $W_{p0} = 9.6 \mu\text{m}$ and $W_{s0} = 11.1 \mu\text{m}$. A pump power of approximately 71 mW is now needed for a 3 dB crystal gain.

In practice the gain formula assumptions such as the signal beam remains Gaussian as it is amplified and all stimulated photons add to this beam will not be met. The pump powers calculated here should be considered absolute minimums for the ideal conditions assumed, and in practice one should expect to need a larger pump power to obtain the equivalent gain.

c. Index Guided Amplifier

For this scheme we assume a single mode fiber whose core is an active gain medium. One such possibility would be a short section of glass fiber with a Nd:glass core. Because of its noncrystalline nature this type of fiber could be pulled so that the core region would have a diameter of several microns. This would allow dimensions very similar to existing silica fibers which would eliminate the need for

coupling lenses since the fibers could be butted together.

Since the beams are now guided, their waists will not change with distance. By setting $W_p(z) = W_s(z) = W_0$ where W_0 is the core radius of the fiber amplifier we can integrate Eq. (II-11) to obtain

$$g_0 = \frac{\sigma_s \tau_2 \eta_0}{h \nu_p} \frac{P_p}{\pi W_0^2} \left[1 - e^{-\alpha_p \ell} \right] \quad (II-15)$$

In Eq. (II-15) ℓ is the length of the fiber amplifier. This equation should model the gain more accurately than the previous unguided amplifier schemes since the signal beam will remain Gaussian in nature as it travels along the fiber. The assumption that all stimulated photons contribute to the growth of the signal mode may still be a bit restrictive but one might guess that this would not effect the final result too much.

By making the amplifier length several times larger than the absorption constant (i.e. $\ell \gg \alpha_p$) we find that the gain through the fiber amplifier is independent of the absorption length. This implies that using high absorption materials such as $\text{NdP}_5\text{O}_{14}$ will offer little if any advantage. It turns out that the best materials to use are the ones that have large cross-section lifetime products (i.e. $\sigma_s \tau \rightarrow$ large). It should also be noted that since the gain is independent of the absorption coefficient we are not restricted to using a strong absorption line of the gain medium, as long as the fiber amplifier is sufficiently long to absorb all of the pump, any wavelength will do. This relaxes the constraint of the two earlier amplifier schemes which required specific pump wavelengths which at present are not easily obtainable at the required power levels. This also means that the amount of active atoms (Nd in the case of a Nd:glass core) doped into the fiber core is not important, assuming the fiber is long enough to absorb all of the pump power.

Assuming a Nd:glass core with a $3.5 \mu\text{m}$ radius a pump power of approximately 19 mW is needed to get 3 dB of gain. The pump intensity for this power level would

be about 150 KW/cm^2 which is of the same order of magnitude as the saturation intensity (which depends on the pump wavelength used). Although pump saturation may take place it may not present a loss in gain since the pump power not absorbed due to a saturated medium remains guided and will eventually get absorbed where it can be used to contribute to the signal's amplification.

Nd:glass was used in the above example since it seems feasible to be able to use the same technology as used in the manufacturing of normal single mode fibers. But since the Nd atom is in an amorphous glass structure its gain profile is spread out which results in it having a much lower gain than Nd:YAG which is in the form of a crystal. If it were possible to make a $3.5 \mu\text{m}$ core fiber out of Nd:YAG, only 0.8 mW of pump power would be required to achieve a gain of 3 dB. This amount of power could be easily supplied by a laser diode which would allow for a very efficient all fiber amplifier system.

3. Experimental Results

At present, experimental measurements have used Nd:YAG as the active gain medium with an argon ion laser supplying the pump power at $\lambda_p = 514.5 \text{ nm}$. The signal beam is obtained by a Coherent Inc. YAG-TWO laser operating at a $1.064 \mu\text{m}$ wavelength.

Figure II-5 describes an early attempt in the measurement of crystal gain in a Nd:YAG rod. The pump and signal were combined into the same $2 \mu\text{m}$ (radius) fiber by using a directional coupler as a wavelength multiplexer. This process depends on the fact that the coupling coefficient varies with wavelength, making it possible to couple the pump and signal into the same fiber. The pump and signal beams were then sent through two single element lenses and focused into a 8 mm length rod of Nd:YAG whose end faces were polished and antireflection coated for $1.064 \mu\text{m}$. After passing through the Nd:YAG crystal the unabsorbed pump was eliminated

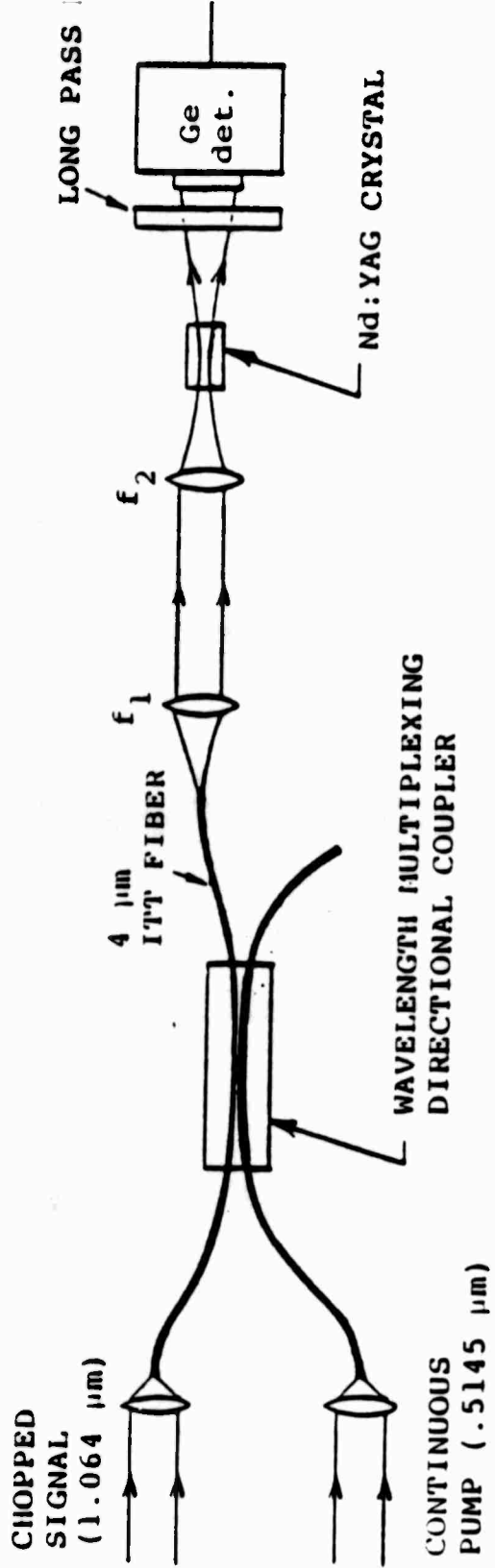


Fig. II-5. Experimental set-up for initial gain measurements.

filters in place the pump signal could be blocked without observing any change in the detector output. To differentiate the signal from the spontaneous fluorescence the signal beam was chopped before being combined with the pump. Since the pump power was continuous the spontaneous fluorescence was constant and could be differentiated from the chopped signal.

To measure the gain the signal was monitored while the Nd:YAG rod was moved into and out of the beam. Initially measurements were attempted by leaving the Nd:YAG rod in the path of the beams and blocking only the pump. This led to poor measurements since the coupling ratio of the signal through the directional coupler was a function of the intense pump beam (several hundred milliwatts) traveling through it. It is believed that the pump power caused local heating in the interaction region of the coupler to effect the coupling of the weaker signal beam. This effect was enhanced by the fact that the $1.064\ \mu\text{m}$ signal was very weakly guided by the $2\ \mu\text{m}$ core fiber which resulted in very large evanescent tails in the coupling region. The effect of the coupling dependence of the signal as a function of the pump power is not serious in an operating amplifier arrangement since the pump signal will be continuous and whatever thermal changes it causes can be removed by readjusting the coupler.

For incident pump powers of up to 200 mW the measured gains in this system were on the order of 10% . This small gain is most likely due to the chromatic aberration of the lenses which causes the pump and signal waists to occur at different locations in the crystal. Although chromatic aberration was expected, simple calculations made to estimate its effect were not accurate since a much larger gain was anticipated.

The next scheme shown in Fig. II-6 consisted of a bulk beam splitter used to combine the pump and signal beams into a common fiber. A single slab ($\ell = .8\ \text{mm}$)

fiber. The detection scheme was identical to that of Fig. II-5 where the signal beam was chopped to differentiate it from the spontaneous fluorescence. The measured gain for this arrangement was only about 30% (1.14 dB) for incident pump powers of approximately 200 mW. This gain of 30% was only achieved when there was a small separation between the crystal slab and the fiber end face. As the crystal and fiber were brought into contact the gain decreased demonstrating the effect of the higher pump intensity saturating the gain medium. Neglecting the saturation effect of the pump, Eq. (II-11), predicts a crystal gain on the order of 4 dB. This dramatic decrease in measured gain can be explained by pump saturation due to the small spot size of the pump ($W_{p0} \simeq 2 \mu\text{m}$) as it leaves the fiber. This small spot size allows for a very short Rayleigh range (i.e. effective interaction length of pump and signal) and then for a large beam divergence which prevents significant gain if the fiber and crystal are not in contact.

The reason these gain measurements were made using such a small core fiber was to ensure that both pump and signal be single mode when leaving the fiber. A larger core would have caused the pump ($\lambda_p = .5145 \mu\text{m}$) to become double mode making the crystal gain a function of the mode structure leaving the fiber. By using a longer wavelength pump (say $\lambda_p \simeq 810 \text{ nm}$) the core size could be increased and the effect of pump saturation would not be so severe. Also, the use of an amplifying medium such as $\text{NdP}_5\text{O}_{14}$ which has a larger pump saturation intensity could make this amplifier arrangement more acceptable.

The last amplifying scheme tested to this date has given the largest crystal gains and is shown in Fig. II-7. The pump and signal beams are combined using a dichroic beamsplitter which transmits 85% of the pump power ($\lambda_p = .5145 \mu\text{m}$) while reflecting approximately 99.3% of the signal ($\lambda_s = 1.064 \mu\text{m}$). The two beams are then focused into a 8 mm length Nd:YAG rod. By using two lenses, one to

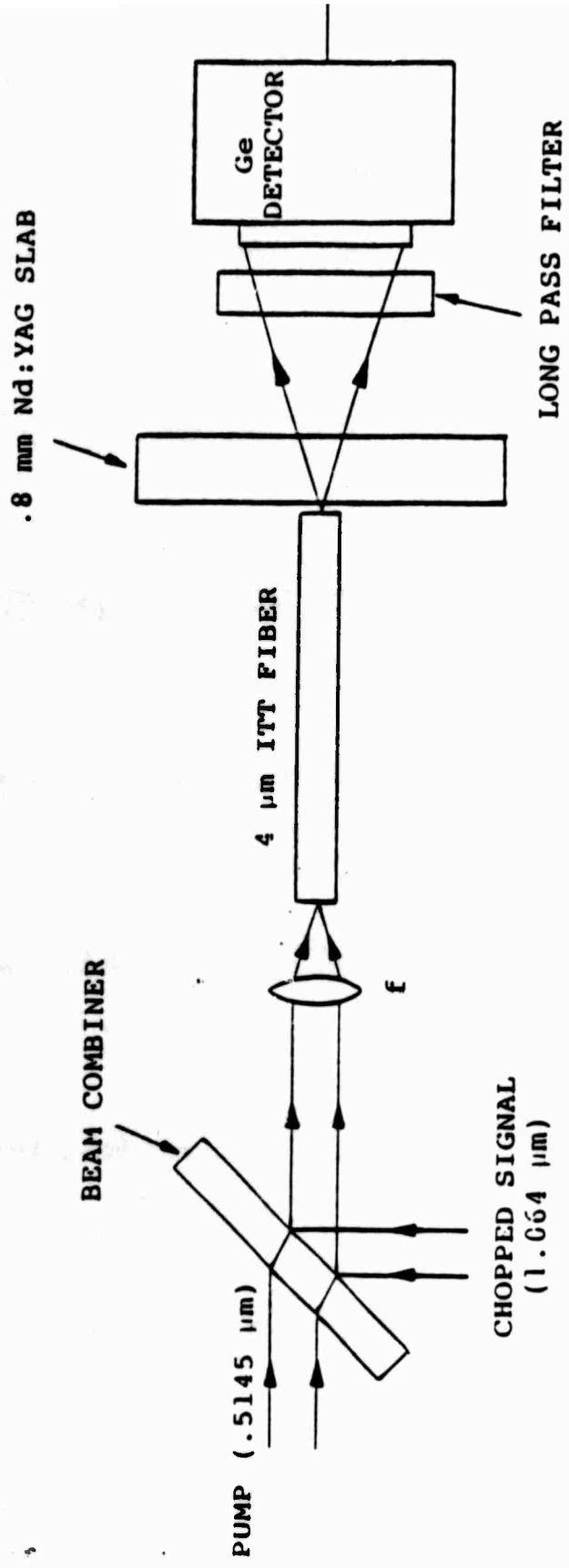


Fig. I-6. Experimental set-up for fiber-slab gain measurements.

collimate the signal and the other to focus the pump and signal into the crystal (see Fig. II-7), it is possible to adjust the location of the two waists in the crystal to achieve maximum gain. The signal beam was chopped before amplification and then detected by a lock-in amplifier after the unabsorbed pump was removed by using a long pass and spike filter.

The Nd:YAG crystal gain versus incident pump power for the arrangement in Fig. II-7 is shown in Fig. II-8. This data shows that to double the signal power (gain of 3 dB) requires a pump power of about 195 mW. The radii of the signal and pump waists in the crystal were measured to be approximately $W_{p0} = 10.2 \mu\text{m}$ and $W_{s0} = 12.4 \mu\text{m}$ and were obtained using $f_1 = 1.8 \text{ cm}$ and $f_2 = 4.6 \text{ cm}$. These sizes were chosen by measuring the gain for various combinations of the two lenses and picking the pair which gave the largest gain. This procedure allowed for maximizing the pump intensity while still remaining below the level where pump saturation decreases the gain.

It is interesting to note that the crystal gain is linear with pump power and not exponential as predicted by earlier theory. This was first thought to be due to either pump or signal saturation but in Fig. II-8 the pump intensity at a power level of 200 mW is approximately 120 W/cm^2 which is about 3 times lower than the 380 W/cm^2 saturation intensity, while the signal is more than an order of magnitude below its saturation intensity.

One possible reason for the observed linear growth of the signal is that since the waist of the pump is smaller than the signal the central portion of the signal beam will grow faster than its Gaussian tails. This larger growth near the optical axis will effectively cause the beam's waist to decrease thus allowing diffraction to come into play earlier causing the beam to diverge. Since the beam diverges sooner due to nonuniform growth along its cross-section the effective interaction region is shortened. This effect could possibly result in a linear instead of exponential growth.

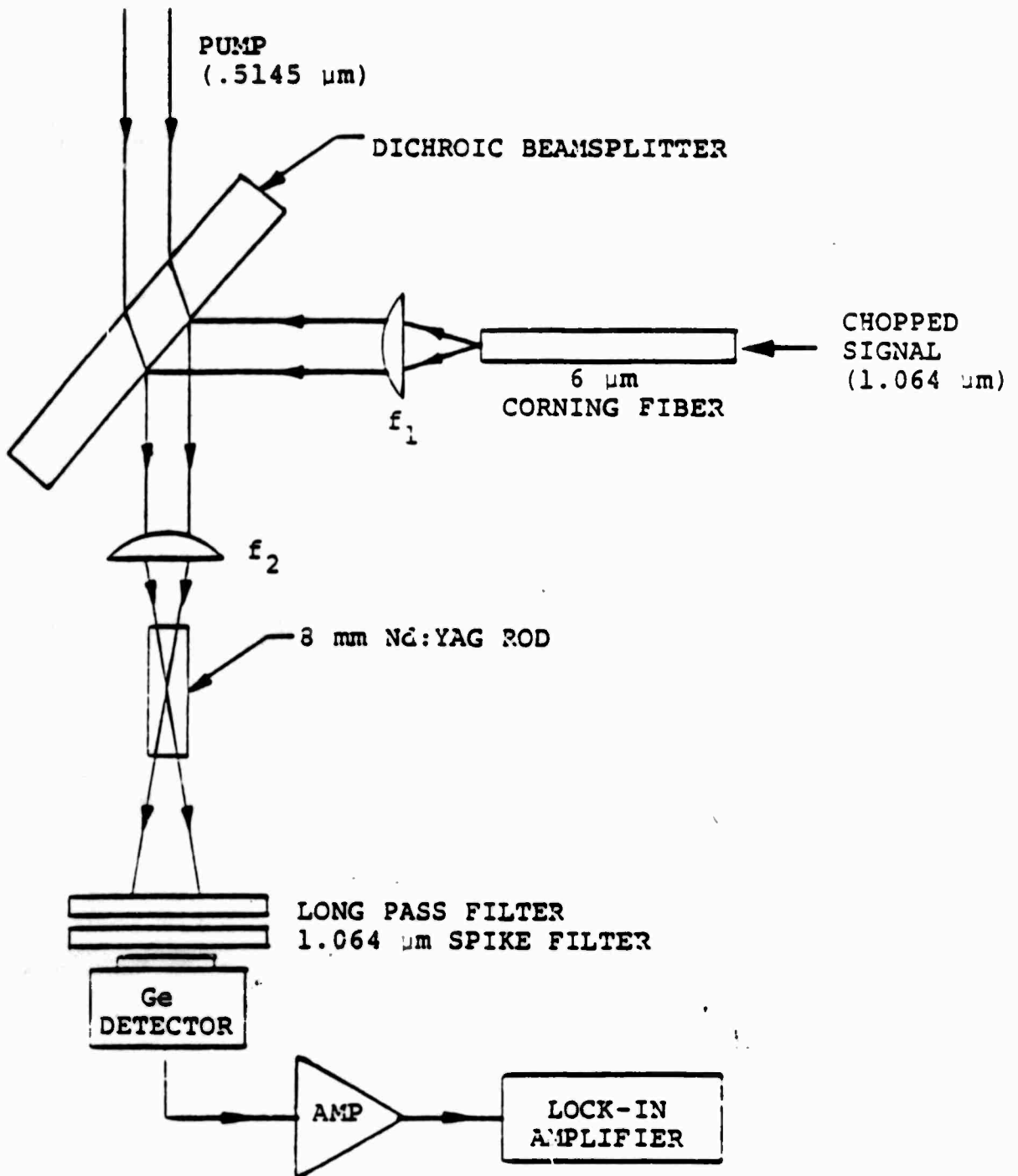


Fig. II-7. Most recent set-up for gain measurement in single rod amplifier.

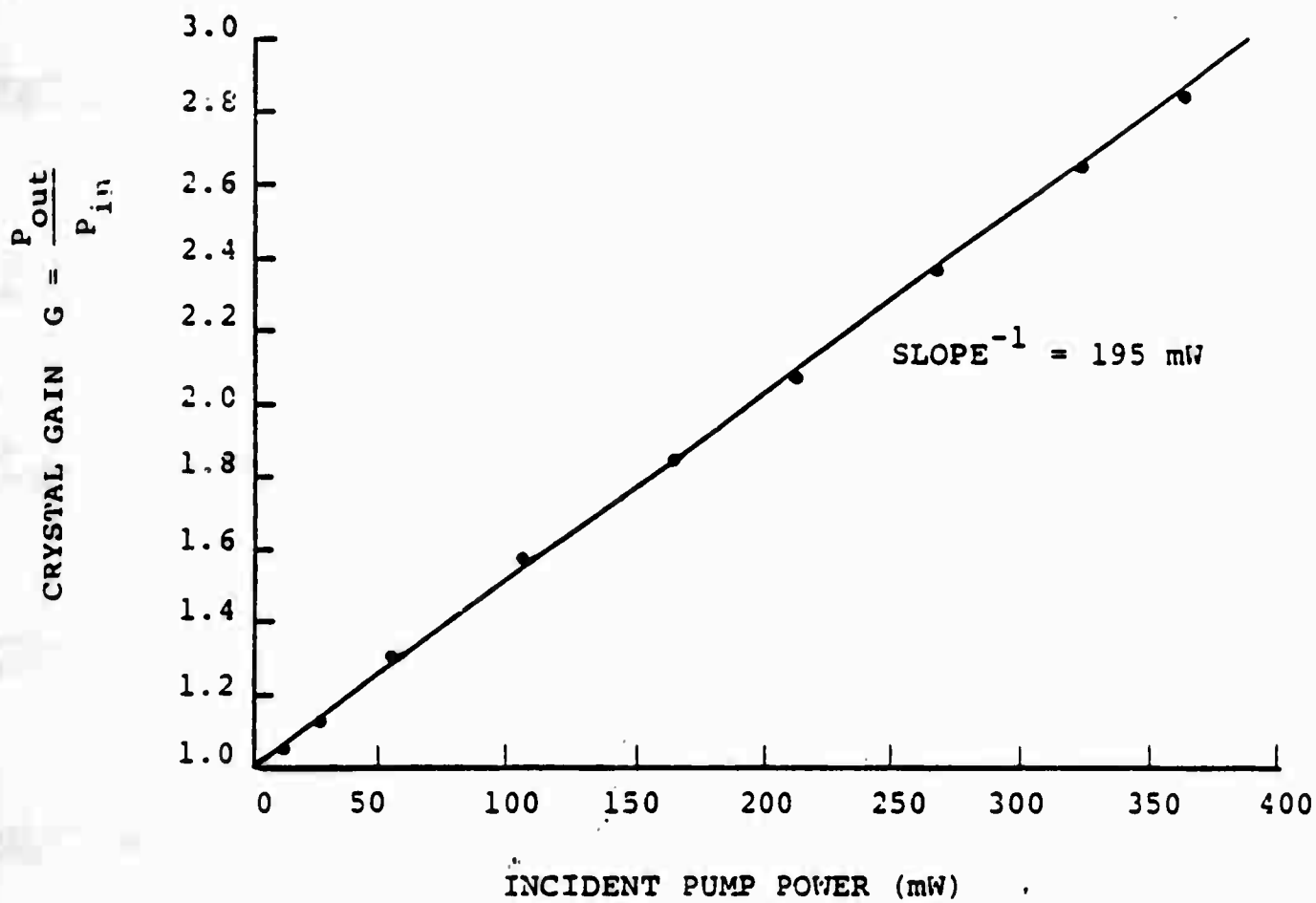


Fig. II-8. Measured gain in unguided 8 mm Nd:YAG rod amplifier. $W_{po} = 9.3 \text{ um}$, $W_{so} = 12.3 \text{ um}$, $\lambda_p = .5145 \text{ um}$.

At present we are not sure whether this diffraction effect alone or a combination of diffraction and saturation is responsible for the nonexponential growth of the signal, a more detailed theoretical analysis is needed to describe these effects. If this diffraction effect is found to be dominant it would violate the assumption used in Eq. (II-12) that the signal beam maintains its incident mode characteristics during amplification.

Equation (II-12) could still reasonably describe the curve in Fig. II-8 if we consider the small gain regime where the experimental curve can be approximated by a linear function. In this regime any diffraction effects due to uneven signal growth should be minimized and therefore not violate the assumption used to obtain Eq. (II-12). The inverse slope from Fig. II-8 is equal to 195 mW while the theoretical small gain regime using Eq. (II-12) gives an inverse slope of 190 mW. Within experimental error this comparison with theory is in good agreement and demonstrates the validity of Eq. (II-12) if gains are not too large. Although experimental results may agree for small gains the fact that the amplification grows linearly instead of exponentially will result in pump powers much larger than previously predicted to get useful crystal gains of 4 or 5 dB.

Recently we were able to obtain some small samples of $\text{NdP}_5\text{O}_{14}$ from W. K. Zwicker at Philips Laboratory. These crystals differ from Nd:YAG by the fact that the Nd atom is a natural part of the crystal structure opposed to being a substitutionally doped atom. This results in Nd concentrations being approximately 30 times larger in $\text{NdP}_5\text{O}_{14}$ as compared to Nd:YAG.

Figure II-9 shows an absorption spectrum through a 1.05 mm piece of $\text{NdP}_5\text{O}_{14}$. For comparison purposes an absorption spectrum through a 6 mm piece of Nd:YAG is shown in Fig. II-10. The $\text{NdP}_5\text{O}_{14}$ shows a much stronger absorption than Nd:YAG, for example at $\lambda = .5145 \mu\text{m}$ the Nd:YAG has an exponential absorption coefficient of approximately $\alpha_p = .7 \text{ cm}^{-1}$ compared to $\alpha_p = 14 \text{ cm}^{-1}$ for

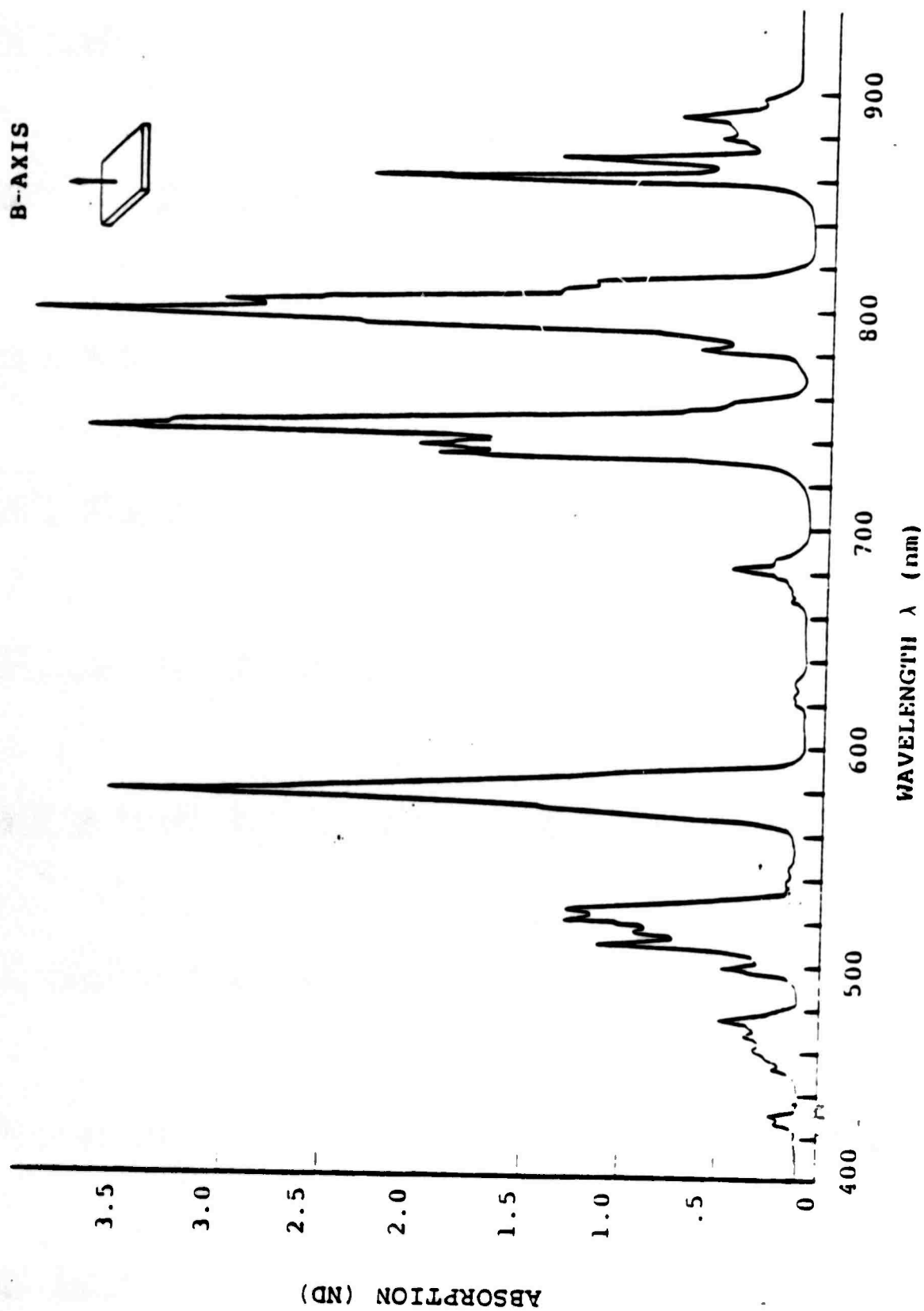


Fig. II-9. Absorption spectrum of neodymium pentaphosphate (NdP₅O₁₄) along its b-axis, thickness = 1.05 mm.

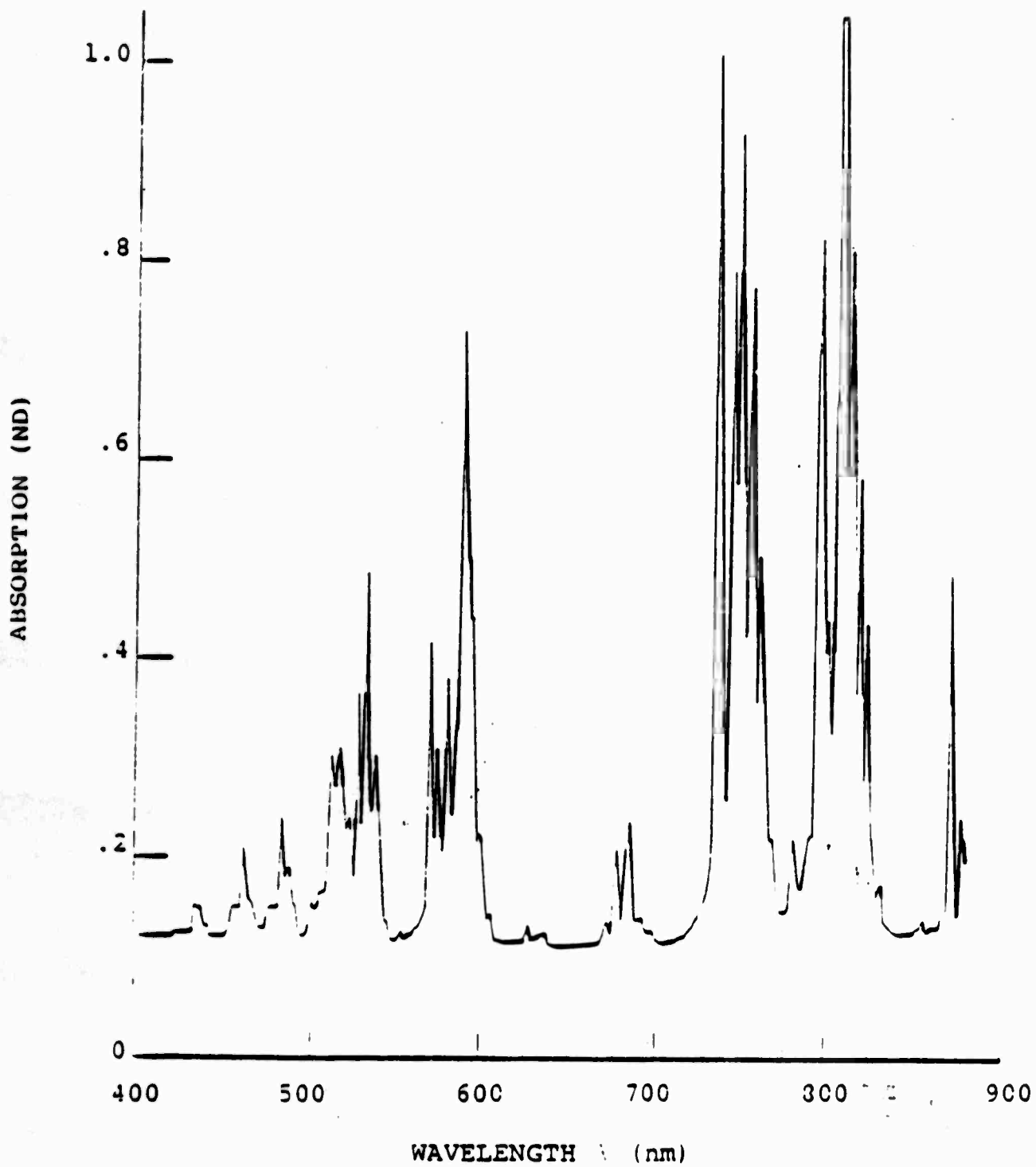


Fig. II-10. Absorption spectrum of Nd:YAG, thickness = 6 mm.

$\text{NdP}_5\text{O}_{14}$. This stronger absorption can contribute to higher gains in unguided amplifier configurations as shown by Eq. (II-11). It can also be noticed that the absorption peaks are slightly shifted, for example the maximum absorption in Nd:YAG occurs at approximately 808 nm while in $\text{NdP}_5\text{O}_{14}$ it occurs at 800 nm. This implies that a pump source optimized for Nd:YAG will not be optimum for $\text{NdP}_5\text{O}_{14}$.

No experimental gain measurements have yet been made with the $\text{NdP}_5\text{O}_{14}$ crystals. These measurements are planned to be carried out soon which will determine the advantages if any in using $\text{NdP}_5\text{O}_{14}$ as a gain medium.

4. Conclusion

Theory shows that due to diffraction of the optical beams the most efficient amplifier scheme consists of a guiding structure to confine the pump and signal to produce large intensities over long interaction regions. Because of the technological difficulties involved with developing such guiding structures initial amplifier attempts have consisted of focusing the pump and signal beams collinearly into a crystal gain medium. Linear growth of signal power versus pump power has been observed in a Nd:YAG crystal with incident pump powers of 195 mW (at $\lambda_p = .5145 \mu\text{m}$) required to achieve a 3 dB gain through the amplifying medium. This linear growth as opposed to the expected exponential growth has caused this amplifier arrangement to be less efficient than initially predicted.

The recent arrival of crystals of $\text{NdP}_5\text{O}_{14}$ will permit tests to determine if they can produce more efficient amplification than the currently used Nd:YAG crystals.

B. SPHERICAL ABERRATION FROM SINGLE ELEMENT LENSES

1. Introduction

The single mode optical amplifier schemes presently being tested require the signal beam to leave the fiber where it is then manipulated with lenses. These

lenses focus the signal into the amplifying medium and then finally back into a single mode fiber (see Fig. II-4). This manipulation of the signal produces coupling losses which play an important role in the amplifier scheme since these losses must be compensated by increased gain through the amplifying medium. A possibly more serious consequence is the reduction in signal-to-noise ratio due to signal loss in the presence of the undiminished amplifier noise. This reduction in signal-to-noise ratio will limit the useful number of times an optical pulse can recirculate in an active fiber loop system.

Since normally used lenses have spherical surfaces, aberrations will be present that will effect the quality of the signal beam. To obtain quantitative results on how these aberrations effect theoretical coupling efficiencies a computer program was developed which numerically calculates how Gaussian beams are affected by spherical refracting surfaces.

2. Theory

The ideal lens surfaces required for focusing beams to a diffraction limited spot are in general not spherical. Because of cost and manufacturing difficulties most lenses are made using spherical surfaces. These spherical surfaces produce many types of aberrations of which all are present in a general imaging system.

If an optical beam is aligned along the optical axis of a spherical lens all aberrations except one can be eliminated. The remaining aberration is known as spherical aberration and is due to the outer edges of the lens focusing rays more strongly than its central region. This effect only becomes significant when the light rays are bent by relatively large angles at the refracting surfaces, which is the case when light is focused into single mode fibers using a single element lens. Because of the small core size associated with single mode fibers, incoming parallel rays must be bent on the order of several degrees which is enough to produce substantial coupling

losses due to spherical aberration. Another way of looking at these losses is that the single mode characteristics of a lowest order Gaussian beam that passes through a spherical lens is disturbed so that some of the beam's energy is distributed into higher order Gaussian modes which can no longer be used when coupling this lowest order Gaussian beam into a single mode fiber.

Because of the nature of this problem an analytical solution describing the magnitude of these losses is not possible. A combination of ray tracing and overlap integrals must be performed to compute the effect of these losses when focusing with spherical lenses.

The computer program developed to do this assumes that both input and output beams are Gaussian and calculates a mode overlap to determine the power transferred between these modes. Like in the previous amplifier section if we make the assumption that the single mode fibers propagate a Gaussian mode (this approximation is good to within a few percent in most single mode fibers) this program can be used to calculate coupling efficiencies into single mode fibers.

The program operates by first analytically projecting an input Gaussian beam onto the first surface of the lens, it then determines the beam's plane wave Fourier components whose amplitude, phase and angle of propagation are stored for later processing. Using Snell's law the angular deviation of the beams Fourier components are calculated and this information is used to project these Fourier components onto the second surface of the lens. The accumulated phase of each Fourier component is computed to provide information on both the amplitude and phase distortion caused by the spherical surfaces. At the second surface Snell's law is again used to calculate the parameters of the input Gaussian beam as it just leaves the lens. At this final surface a mode overlap integral is performed between the beam leaving the lens and the required Gaussian beam needed for 100% coupling into the single mode fiber. Since the projection of the desired beam for 100% coupling depends

on the fiber-lens distance the computer must vary this fiber-lens distance until a maximum coupling efficiency is obtained.

The above description uses a ray optics approach to determine how the input Gaussian beam is affected by the spherical surfaces of a lens, this approach neglects any diffraction effects on the beam as it propagates through the lens. Since beam diameters will be on the order of millimeters or greater while propagating through the lens any diffraction effects over the thickness of a lens should be negligible. However, diffraction effects are taken into account when the Gaussian beams are analytically projected onto the lens surfaces.

The above program combines ray tracing with coherent Gaussian beam wavefronts to determine coupling losses due to both amplitude and phase distortions from spherical surfaces used in focusing. Examples showing the order of magnitude of these losses are given in the following section.

3. Results

The following examples are all concerned with coupling losses when using single element lenses. Although the program is not limited to two surfaces per lens, these single element lenses are commonly used in laboratories and information on their focusing ability should be useful.

Figure II-11 models the situation where a collimated Gaussian laser beam is focused to a small spot with the use of a single plano-convex lens. Although the plano-convex lens does not have the correct spherical surfaces to minimize spherical aberrations (for the given focusing arrangement) it is very close and is commonly used to focus collimated input beams. To minimize aberrations this lens is situated so its curved surface faces the incoming parallel beam (see Fig. II-11), this allows the input and output rays to make approximately the same angles with the lens surfaces which reduces the overall focusing error since this error has a nonlinear

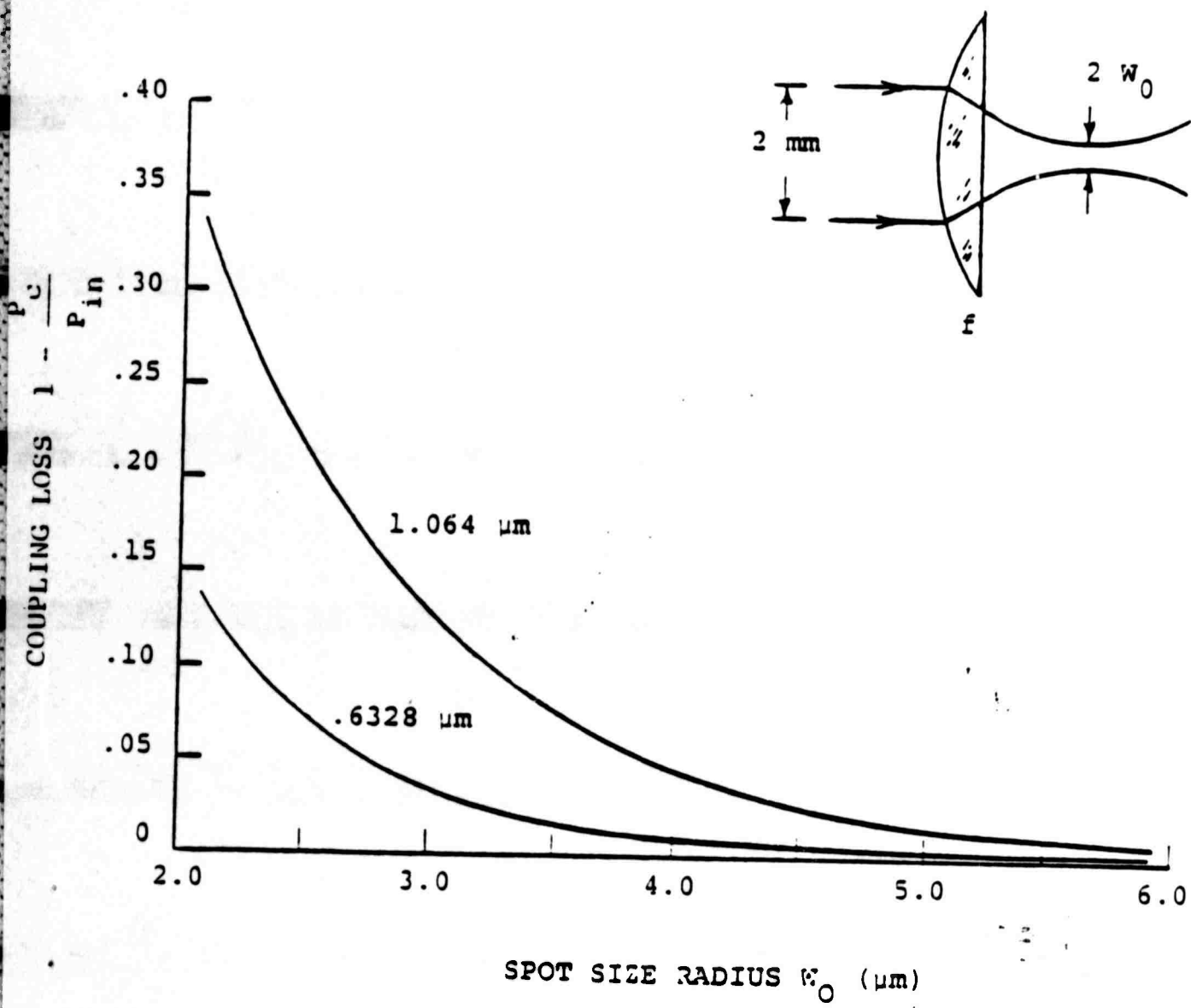


Fig. II-11. Fractional coupling loss due to mode mismatch caused by spherical aberration. Lens focal length is adjusted according to paraxial theory.

Reproduced from best available copy.

dependence with angle.

The input in Fig. II-11 is assumed to be a collimated Gaussian beam with a 1 mm radius (measured to the 1/e point in field amplitude). Using paraxial ray theory the required lens focal length and curvatures are analytically calculated to focus the input beam into the desired spot size. Once these parameters are known the program then calculates the coupling efficiency between the beam leaving the lens and that needed to produce the desired spot size. This is then assumed to approximate the coupling efficiency into a single mode fiber with the equivalent spot size for its guided mode. Losses due to other sources such as reflections have not been included, therefore the plotted loss is due solely to the mismatch between modes caused by the spherical lens surfaces.

The top curve in Fig. II-11 shows the coupling loss if the incoming beam is from a Nd:YAG laser ($\lambda = 1.064 \mu\text{m}$) while the bottom curve is for the commonly used helium neon laser ($\lambda = .6328$). The larger coupling losses for the Nd:YAG wavelength is due to diffraction effects which increase with longer wavelengths.

In our Lab a commonly used fiber with helium neon lasers has a core radius of 2 microns. From the bottom curve in Fig. II-11 one can see that the mode mismatch losses are on the order of 15%. If the three reflection losses (two from the lens and one from the fiber face) are taken into account this implies the maximum coupling efficiency into the single mode fiber is on the order of 75%. This assumes perfect spherical surfaces, ideal alignment and a correctly chosen focal length which means in practice the coupling will be much lower. A fiber commonly used in our lab for guiding $1.064 \mu\text{m}$ radiation has a $3 \mu\text{m}$ core radius. The top curve in Fig. II-11 shows a mode mismatch of 13% for this fiber which results in approximately the same coupling efficiency as the above helium neon example. The amount of computational time required to generate each curve in Fig. II-11 was approximately one hour (the program was written in Basic and run on an HP9826 desktop computer, each curve

consists of 50 calculated parts).

Figure II-12 shows the extra losses that can occur if a bi-convex instead of a plano-convex lens is chosen to focus the same input Gaussian beam. Bi-convex lenses are best suited for one to one imaging, therefore when attempting to focus an incoming planar beam they show much more spherical aberration than the better suited plano-convex lens. The two curves are plotted for $1.064 \mu\text{m}$ radiation following the same conditions given in Fig. II-11. If a bi-convex lens was used to focus the input beam into a 3 micron core there would be an 8% increase in loss compared to the plano-convex lens. By observing the tails of the curves in Fig. II-12 one can see the losses for the bi-convex lens are more than twice that for the plano-convex lens, only when losses become greater than about 5% does the relative difference in losses decrease.

To obtain an estimate for how losses are effected by scaling up the dimensions of the focusing elements Fig. II-13 was plotted. For this curve the focused spot size was kept constant at a radius of $3.2 \mu\text{m}$, this is approximately the mode size for $1.064 \mu\text{m}$ radiation in the Corning $6 \mu\text{m}$ (core diameter) fiber used in our lab. With the focused spot size fixed the radius of the incoming collimated Gaussian beam was varied. To focus to the fixed spot size paraxial theory was used to adjust the focal length and curvature of the plano-convex lens to provide mode matching (to first order).

By increasing the diameter of the incoming beam we are effectively scaling up all the dimensions of the imaging system while keeping the image size constant. As Fig. II-13 shows, the losses increase approximately linearly with increasing beam and lens sizes. This effect can be understood by noting that as the input beam increases the lens focal length must increase. This means that although the angles bent by the incoming rays remain constant any angular errors are translated into much large transverse offsets at the location of the spot size since the distance they

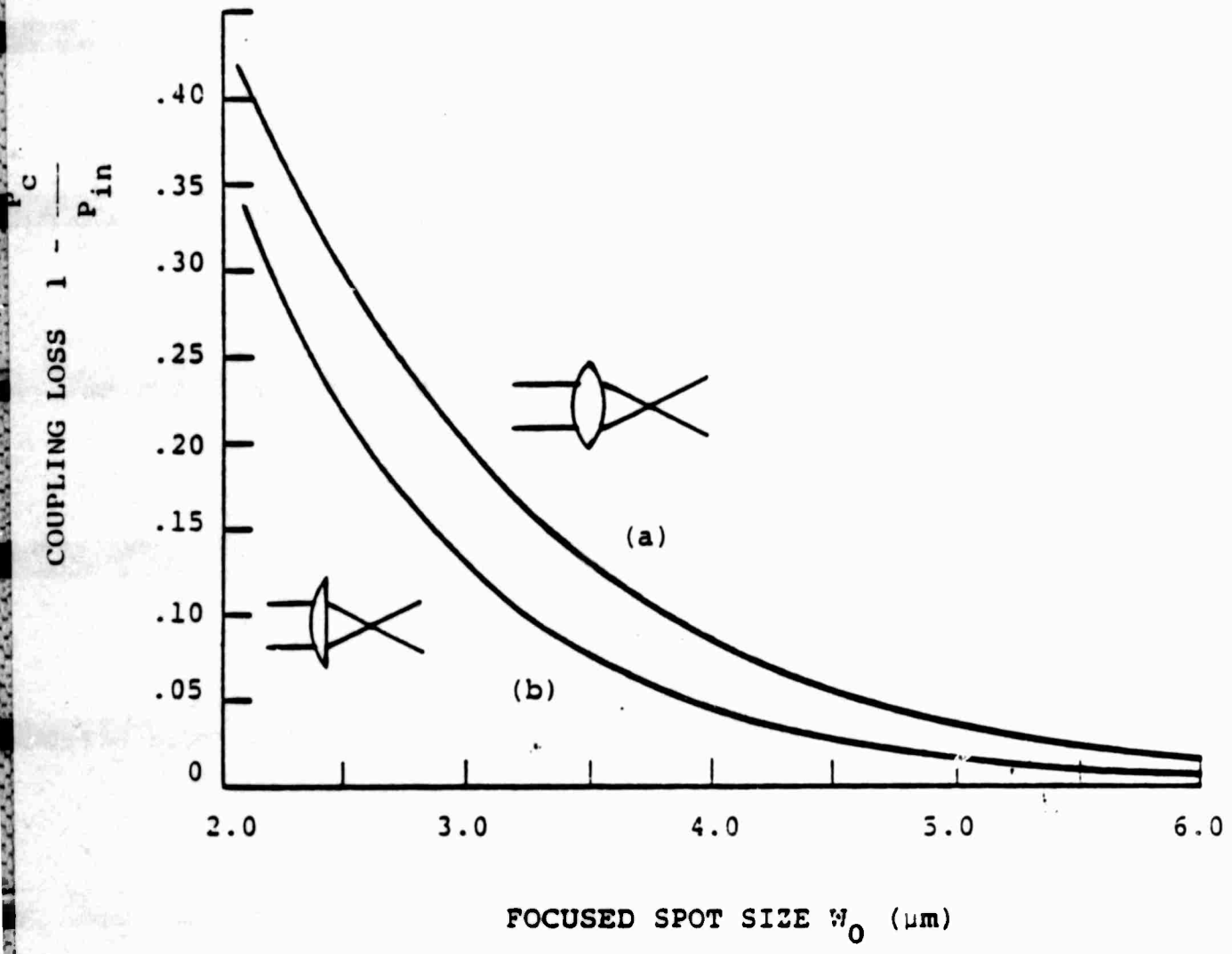


Fig. II-12. Comparison of spherical aberration between a (a) bi-convex and (b) plano-convex lens. Radius of input beam is 1 mm, and wavelength = 1.064 μm .

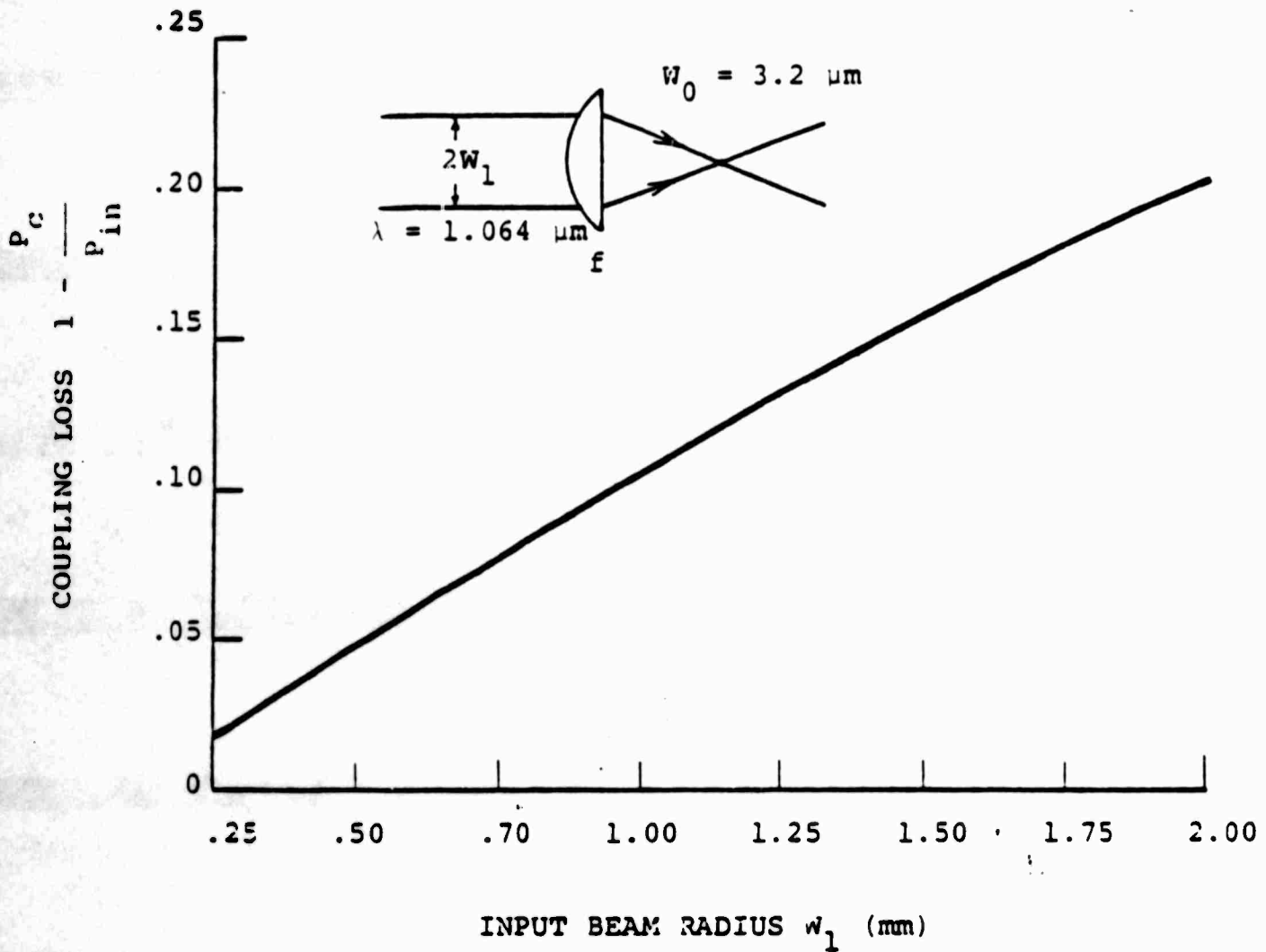


Fig. II-13. Coupling loss of plano-convex lens as radius of input beam is varied. Focused spot size is fixed at $w_0 = 3.2 \mu\text{m}$. Lens focal length is adjusted according to paraxial theory.

must travel increases. This explanation implies that one would expect the coupling losses to increase in an a linear manner with increasing focal length (i.e. input beam size) as shown in Fig. II-13. These results imply that when focusing beams from one fiber to another it is advantageous to use short focal length optics so that the small constant angular errors at the refracting surfaces are not transformed into large transverse variations at the focused spot.

In the preceding figures the focal length of the lenses were calculated using paraxial theory which assumes that all rays make small angles with the optic axis. It was then assumed that these focal lengths produced maximum coupling into the given spot size. Due to spherical aberrations this assumption is not entirely correct and the optimum focal length will differ slightly from that given by paraxial theory.

Figure II-14 shows coupling losses as a function of focal length. In this figure it is assumed that a 1 mm (radius) input beam of $1.064 \mu\text{m}$ radiation is to be focused into a $3.2 \mu\text{m}$ radius spot. With input and output beams held constant the maximum coupling efficiency was found for each change in the focal length. The resulting curve in Fig. II-14 shows that the minimum coupling loss occurs for a focal length of approximately 10.3 mm which is about 10% larger than the 9.45 mm predicted from paraxial theory. The difference in losses for these two lenses is only about 1% meaning the focal length calculated using paraxial theory provides a coupling which is not too far from the optimum.

The reason why the optimum focal length is larger than that predicted by paraxial theory can be understood by recalling that spherical aberration is the result of the outer edges of the lens having a shorter focal length than the paraxial value. It then seems reasonable to believe that to compensate for the tighter focusing at its outer edges of the lens the focal length should be increased as indicated in the results from Fig. II-14.

To demonstrate how real the effect of spherical aberration can be in a single

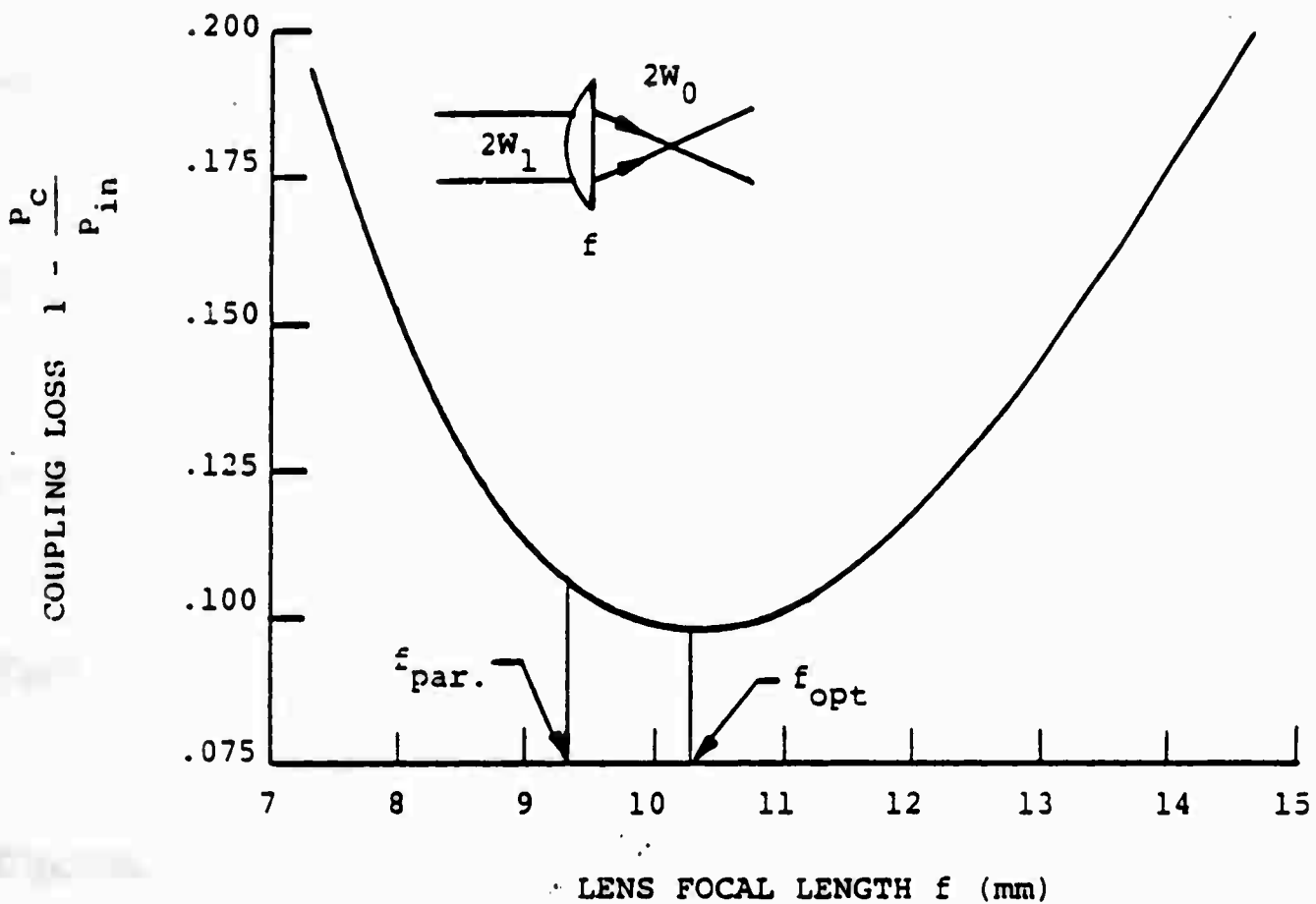
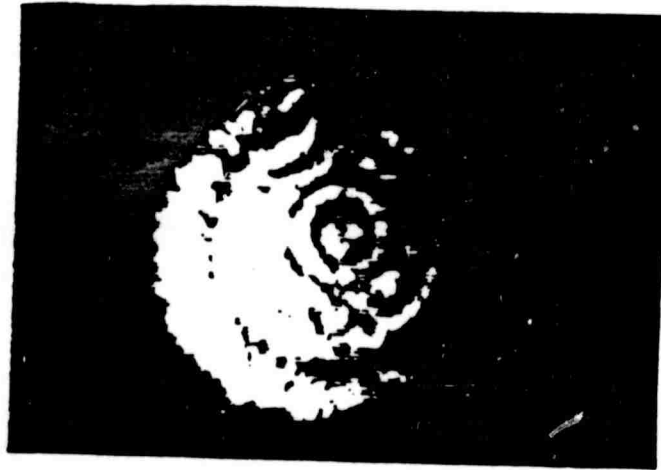
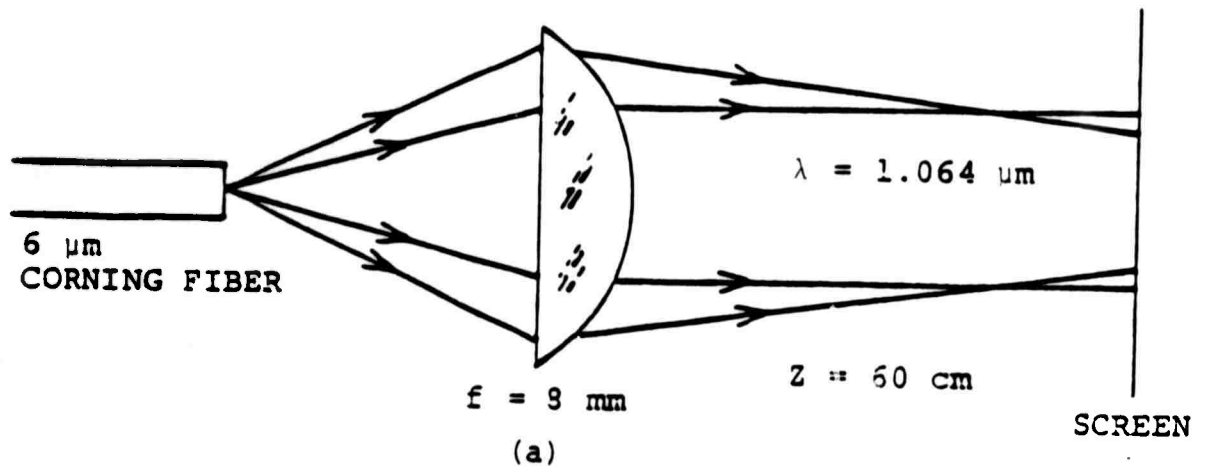


Fig. II-14. Coupling loss due to incorrect focal length. Beam waists are fixed at $W_1 = 1$ mm, and $W_0 = 3.2$ μ m. Wavelength = 1.064 μ m. $f_{par.} = f_{0}$ focal length predicted by paraxial theory. f_{opt} = optimum focal length when spherical aberration is considered.

element lens the output of a single mode fiber ($\lambda = 1.064 \mu\text{m}$, core diameter = $6 \mu\text{m}$) was collimated by a 8 mm focal length plano-convex lens and projected onto a screen. The resulting pattern was not the expected Gaussian intensity profile but a series of rings whose central portion would be either bright or dark depending on how collimated the beam was. Figure II-15 shows some photographs of these rings taken off a cathode ray tube from a closed circuit infra-red T.V. system. Although the contrast between rings in the photographs appears poor this is due to the infra-red T.V. imaging system. When these rings were viewed using a hand held infra-red viewer one could see that the rings were intensity modulated at 100%.

These rings are due to the outer edge of the lens slightly focusing the beam while the central portion collimates it. If one then observes the beam at a sufficient distance from the lens the rings will occur due to an interference effect between the focused and collimated portions of the beam (see Fig. II-15). These ring patterns vividly demonstrate the short comings of using single element lenses when manipulating beams from single mode fibers.

The final example demonstrates the losses involved in coupling light from one fiber to another with the use of a single bi-convex lens. The fiber was assumed to be guiding $.6328 \mu\text{m}$ radiation with a spot size radius of $2 \mu\text{m}$. The output fiber was placed at a distance of 9 mm from the principle plane of a 4.5 mm focal length lens. This separation is the value predicted from paraxial theory to in order achieve a image with unit magnification. The program then varied the receiving fiber-lens distance and calculated the corresponding coupling efficiencies. Figure II-16 shows that the maximum coupling efficiency due just to spherical aberrations is on the order of 35%. It also shows that the maximum power is coupled when the lens-fiber distance is about .18 mm smaller than that predicted from paraxial theory. A shorter image distance is expected since the outer edges of the lens focuses the beam more strongly. Similar results (i.e. 36% coupling efficiency) were obtained



(b)



(c)

Reproduced from
best available copy. 

Fig. II-15. Projection of collimated beam from single mode fiber. (a) Arrangement of plano-convex lens for collimating beam. $W_0 = 3.2 \mu\text{m}$ at fiber face. Wavelength = $1.064 \mu\text{m}$. (b) Ring pattern on screen. Diameter = 6 mm. (c) Ring pattern for fiber slightly backed off. Diameter = 2 mm.

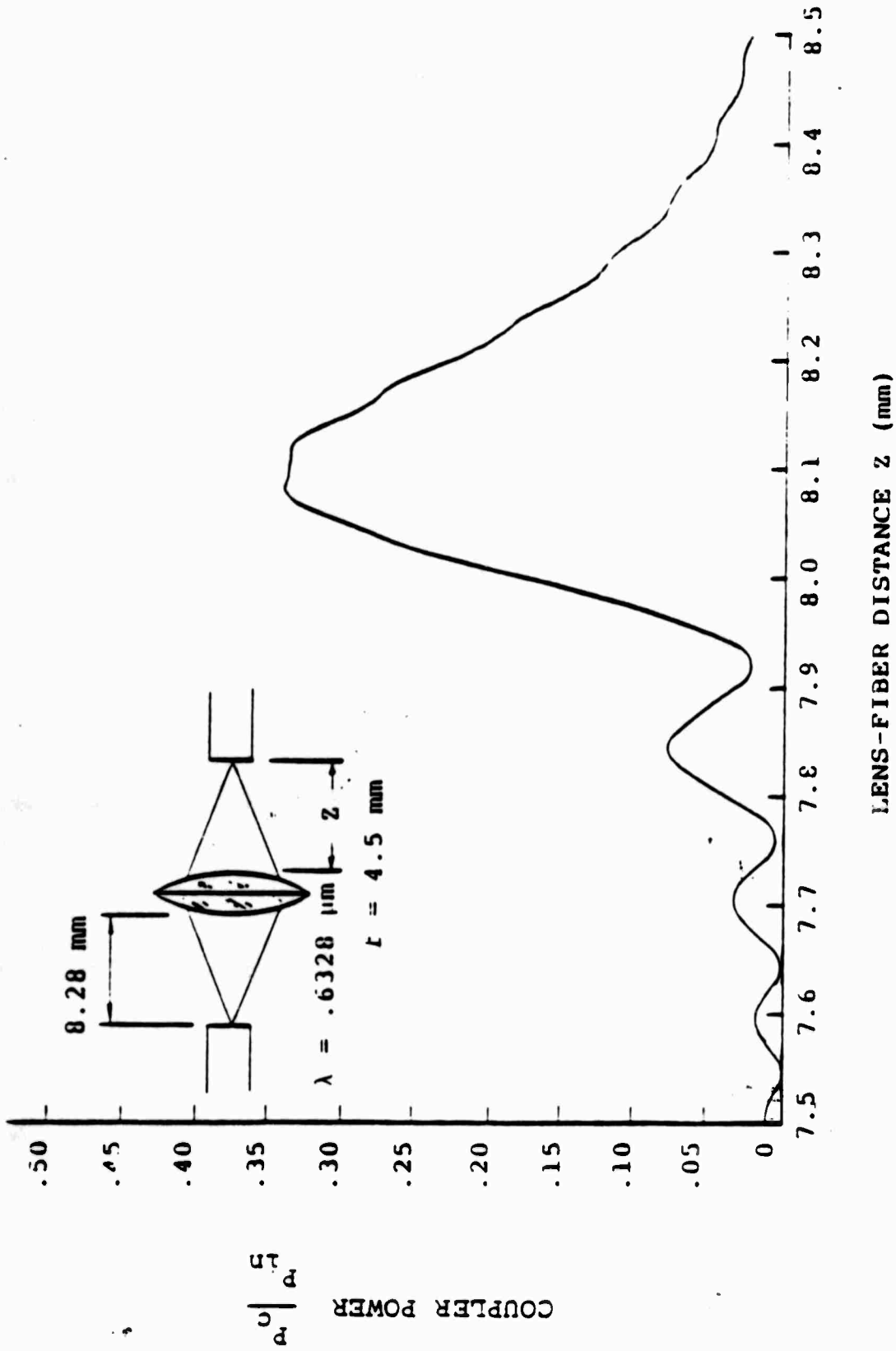


Fig. 11-16. Fiber to fiber coupling efficiency using a single bi-convex lens. Lens-fiber distance is measured from lens surface to fiber face. Fiber core is assumed to have a 2 μm radius.

using a $1.064\ \mu\text{m}$ wavelength and a $3\ \mu\text{m}$ radius core size.

Figure II-16 also shows a ringing type of response for its coupling efficiency at distances slightly shorter than the optimum focusing distance. This ringing structure is the result of local high and low intensity points along the optic axis, these same effects are shown in the photographs of Fig. II-15 where a fiber output is collimated onto a screen.

The results of Fig. II-16 show that losses due to spherical aberrations of a single element lens can be very large when dealing with diverging beams from single mode fibers.

4. Conclusion

It has been shown that the mode mismatch losses due to spherical aberration in single element lenses is very large when dealing with diverging beams from single mode fibers. The net coupling into a fiber also depends on such factors as reflections, surface imperfections, misalignment errors, etc. therefore coupling losses in practice will be larger than those computed for the mode mismatch alone.

Since spherical aberration is a nonlinear function of the refracted angle a ray makes at each lens surface, this loss mechanism can be made arbitrarily small if many surfaces are used so the refracted angle at any one surface is very small. Although many surfaces will decrease mode mismatch each surface will contribute to reflections and surface scattering which implies that the maximum coupling efficiency will be a trade off between mode mismatch and surface losses.

Optimized achromatic doublet and triplet lenses will have much smaller spherical aberrations without too much of an increase in surface reflections. Lenses of this type will be used to find maximum experimental fiber coupling efficiencies to determine their usefulness as components in the bulk crystal amplifier arrangements discussed earlier. Theoretical analysis will also be carried out to determine the

reduction in mode mismatch losses when using these multi-element lenses.

Although the use of single element lenses could have been determined by qualitative analysis, this analysis was pursued to provide quantitative results on the actual magnitude of these losses. The results of this section will also be useful in any other application where single element lenses are used.

III. SOURCE NOISE AND SCATTER LIMITATIONS

A. Introduction

Optical fiber Sagnac interferometer gyroscopes suffer from the backscatter of light in the fiber. Some of the light which returns by scattering from one of the counter propagating waves adds to the other signals coherently but with unpredictable phase, producing error in the measurement of rotation (Cutler 1980, Ulrich 1980, Bohm 2/81, Burns 1983). It has been observed, as predicted, that reducing the temporal coherence (broadening the spectrum) of the light introduced into a laser gyro reduces the error due to the addition of Rayleigh backscatter by reducing the coherence between primary and scattered components (Bergh 1981, Bohm 2/81). Earlier calculations indicated that a coherence length as short as one millimeter (i.e. 300 GHz bandwidth) is required to minimize the error due to coherent backscatter from the middle section of the fiber loop. With careful selection of a laser source and attention to environmental effects, sensitivities close to a limit set by shot noise have been attained.

Generally, the statistical fluctuations in the intensity of optical sources seem not to have been considered as a source of error. The fluctuations, even though reduced by saturation in the source, are not necessarily negligible.

It is the purpose of this section is to analyse the effect of inherent fluctuations in a laser source and of scattering in the fiber on phase measurement in interferometer

systems, and to obtain an evaluation of the error as a function of source coherence and transmission parameters. While the discussion is focused on the Sagnac interferometer (Fig. III-1) having a phase modulation bias in the loop, it may have applicability to optical fiber interferometer systems in general. Both (Rayleigh) backscatter and the statistical (Rayleigh)* source fluctuations are found to be a larger source of error than shot noise in some typical instances.

B. The Effect of Signal Statistics on Optical Fiber Gyros

1. Some Basic Concepts, Coherence

Unfortunately the coherence characteristics of an optical signal usually are not well described by a single number. A multi (longitudinal) mode source with a tendency to mode lock might give a signal with a complicated mix of long and short coherence characteristics. Amplitude fluctuations are not simply related to the observed spectra. The coherence of a signal may be complicated by sensitivity of the source to feedback from reflected waves; and a signal may be random in phase but fixed (saturated) in amplitude. In the following, we consider several possibilities; (1), that the signal has the characteristics of featureless band limited thermal noise, saturated or unsaturated in amplitude; (2), has multi longitudinal, not phase locked, modes nearly approximating the multifrequency Fourier spectrum of band limited white noise; (3), has the uniform amplitude randomly fluctuating phase character of the classical cw electronic oscillator with a finite Q ; or (4), has a number of independent oscillations each like the classical oscillator but in frequency separated channels throughout a wide bandwidth. The latter may be from a homogeneous or inhomogeneously saturating medium or something in between, and may have an overlay of super radiance. It has lately been observed that semiconductor (injection)

* Do not be confused by the two different Rayleigh phenomena. They are distinct.

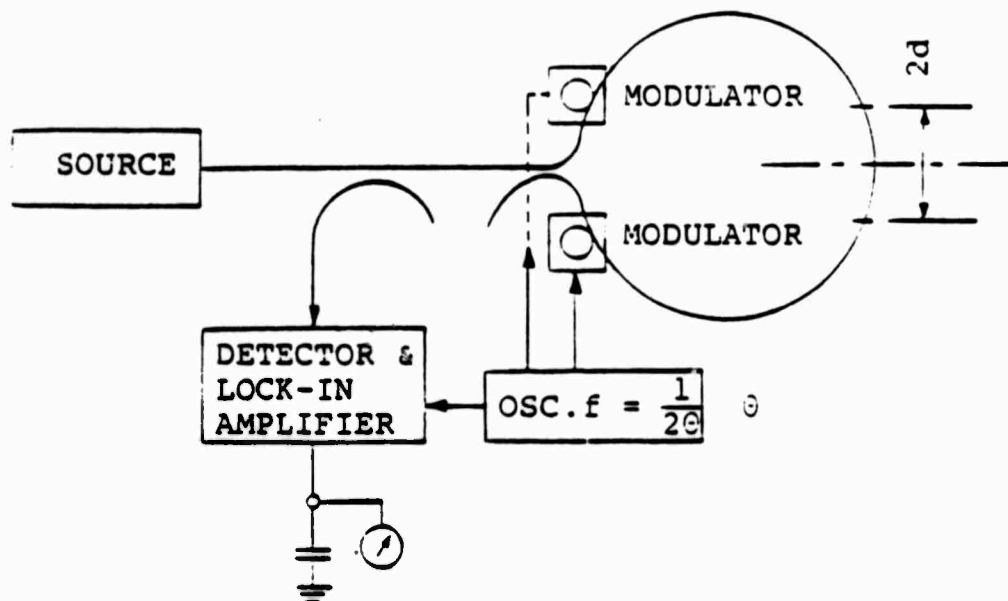


Fig. III-1. Basics for a Sagnac interferometer system. There are four sources of fluctuation (error) in the output: 1. Fluctuations in the source intensity. 2. Interference of backscattered energy which is coherent with the primary wave (i.e., from section $2 \cdot d$ near the loop, where $2 \cdot d = \text{velocity times coherence length}$). 3. Interference of backscattered energy which is not coherent with the primary wave. 4. Shot noise.

lasers evince a signal in which the phase modulation index exceeds the amplitude modulation index by 13 dB (Henry 1981, Peterman 6/81, 4/82, Harder 1983). This fact is crucial to the quantitative evaluation of gyro sensitivities. Many kinds of signals occur in existing light sources and in a variety of combinations. However incoherent the source, the fact that the signal is band limited gives it considerable character.

It is believed that the matters to be discussed are adequately described in classical, (i.e., non-quantum mechanical) terms.

2. Fluctuation in the Primary Signal

An obvious possible cause of fluctuation in any optical transmission system is the inherent fluctuation of the source. If the source has the character of band limited, (not gain saturated) thermal noise like one might obtain from super radiance, we have a case well treated in the literature. (Rowe 1965, Rice 1944, Pierce 1979). The signal is said to have a Gaussian statistical distribution in (instantaneous) amplitude, and a Rayleigh statistical distribution in intensity. Frequently this source of noise is neglected, being smaller than shot noise at low (received) signal levels (Personic 1981). When looking for small phase changes of a strong carrier in an interferometer, it is not likely to be negligible.

From Rice (1944) Eq. (4.55), a high frequency band of noise $W(f)$ has a fluctuation in noise power (base band power spectrum of the fluctuation):

$$W_c(f) = \int_0^{\infty} W(x) \cdot W(x-f) dx \quad (III-1)$$

Where W_c is the power spectral density in the base band at frequency f , derived from the optical power spectrum, $W(x)$. When the spectrum is square, this is (from Rice, or Pierce Eq. 2.5-15):

$$W_c(f) = 2W(B-f) \frac{1}{B^2} \quad (III-2)$$

which gives the mean square fluctuation in base band power as illustrated in Fig. III-2a. A more realistic Gaussian-like or raised cosine high frequency spectrum also gives an approximately triangular spectrum with a maximum fluctuation at zero frequency.

Roughly, when $f \ll B$, letting $\tau = 1/B$:

$$W_c(f) \simeq 2\psi\tau \text{ per cycle of base band width} \quad (III - 3)$$

Where $\psi = \xi G^4$, G^2 is the optical signal power, ξ is a conversion and efficiency factor to account for loss in the detector, and τ is the coherence time or the reciprocal bandwidth $1/B$ of the signal. With increasing f , $W_c(f)$ tapers to zero at $f = B$, but we only care about the fluctuations that pass a post detection filter at $f \ll B$.

If the integration time of the detector is t_2 (i.e., post detection filter band width $= B_0 = 1/t_2$) we have:

$$\frac{\text{fluctuation}}{\text{dc output}} = \sqrt{2t/t_2} = \sqrt{2B_0/B} \quad (\text{optical power ratio}) \quad (III - 4)$$

This gives the ac fluctuation for the signal incident on the detector at low-frequency band B_0 . For an optical signal with a 1 picosecond coherence time and a one second integration time, this gives:

$$\text{Fluctuation} = \sqrt{2} 10^{-6} \psi \quad \text{watts} \quad (III - 5)$$

that is, 58.5 db below the average optical power level. Because of the ac bias modulation generally used in a Sagnac interferometer, we are interested in the fluctuation in the output, narrow band filtered at a few hundreds of kHz. This is high enough to be clear of the usual $1/F$ noise in electronic systems and common in laser fluctuations but is low enough so that the approximations used in Eq. (III-3) are reasonable. This fluctuation is 20 times greater than a typical value

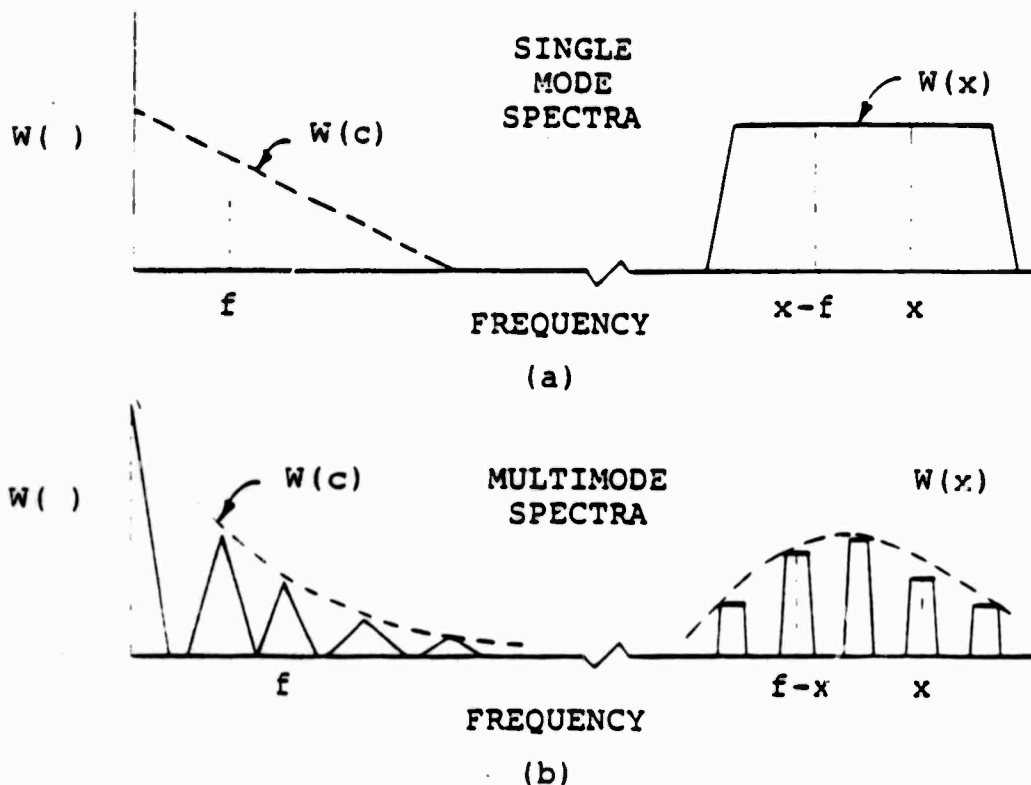


Fig. III-2. (a) Power spectra. A wide bandwidth high frequency noise-like signal begets a triangular spectrum of intensity fluctuation. The value of $W(c)$ depends critically on the phase relations in the high frequency spectra, however, and because of gain saturation the fluctuation may be much smaller than this figure (a) implies. (b) The power spectrum of a multimode source consists of many products spaced by frequency intervals equal to the reciprocal of the round trip transit time of the optical resonator, giving rise to a serrated intensity spectrum at low frequencies. If the medium saturates inhomogeneously, the individual optical modes saturate independently, so the low end of the baseband is subdued.

of shot noise with $\xi G^2 = 10^{-4}$ watts average power into the detector (see the Appendix) and is quite consistent with observations on a laser operating at threshold (Yee, 1983). In a laser, or even in some so-called super-radiant sources, amplitude saturation is evident and a much smaller fluctuation is obtained. If the saturation is homogeneous, the uniform amplitude comes from compensating fluctuations in different parts of the band and any change in the balance of amplitude or phase vs. frequency in the band width would degrade the compensation, leaving stronger fluctuations (partition noise). If the saturating medium is inhomogeneous, sections of the band saturate independently and less low frequency fluctuation would be expected from partitioning of the signal. It appears that most optical sources do operate with a saturated intensity; and multimode sources are at least spatially inhomogeneous. Thus, normal fluctuations in a well behaved optical source are likely to be very much smaller than calculated here. It appears that in semiconductor lasers, the large spectrum line width is due to carrier density changes affecting the index of refraction, or to spontaneous emission events which discontinuously alter the phase and intensity of the lasing field. The spectrum character is mostly due to phase fluctuations. The amplitude fluctuation is smaller typically by a factor of 5 and tends to be white (Peterman 12/81 and 4/82, Henry '82, Harder 1983). This would leave us with a fluctuation level 71.5 db/Hz below dc for a semiconductor laser signal, close to the expected shot noise in a 1 Hz bandwidth. Clearly, saturation clamping of the fluctuation in sources for optical sensors is vital.

Suppose we have a finite number of longitudinal modes of oscillation in the source, typically between 10 and 100. The optical spectrum might cover a wide bandwidth, but with energy concentrated in narrow bands at frequencies determined by the source dimensions, $c/2nL$ where L is the source resonator length and n is the index of refraction. In most respects this signal is the same as band limited noise covering the same band, provided the modes are independent (not locked).

Many modes, randomly phased, yield a Rayleigh distribution of signal amplitude, as before. The optical spectrum, now having a multitude of components, produces a multitude of baseband components, as illustrated in Fig. III-2b. Without a precise knowledge of the source spectrum, we cannot predict the output fluctuation, but perhaps we can deduce some limits.

At one extreme, the phases might be locked, producing a series of pulses with a regular period determined by $2nL/c$ in the laser, and the spectrum components would combine to give baseband components at precise multiples of the pulse rate. Low frequency fluctuations due to shot noise and unspecified factors would result in a secondary sideband structure and some low frequency components; but most of the energy would be in components at multiples of the pulse rate, and not near dc.

If the source has within it a guiding medium with significant dispersion, the longitudinal laser modes are separated by different amounts and are not phase locked. The baseband components produced by beating are separated in frequency because of the multiple values of $Nc/2nL$, but contributions smaller than $c/2nL$ derive from the spectrum width of the individual spectrum components in the same manner as described in the previous section. If there are the equivalent of N equal amplitude modes, each B' Hz wide and having the character of noise, we have for the baseband power spectrum of the fluctuation (using (III-2)):

$$\text{fluctuation power} \simeq W_c(f) = 2 \sum_n \frac{\psi}{N^2} (B' - f) \frac{1}{B'^2} \frac{1}{t_2} \quad (\text{III} - 6)$$

giving;

$$W_c(f) = 2N \frac{\psi}{N^2} \frac{B' - f}{B'^2} \frac{1}{t_2} \simeq \frac{2\psi}{NB'} \frac{1}{t_2} \quad (\text{III} - 7)$$

where B' is the bandwidth of each of the N individual spectrum components. Measurements in our laboratory, and published data (Epworth 1982 or Peterman, 1/82) give $NB' \simeq 10^{11}$ Hz (Fig. III-3), and thus a fluctuation/dc output ratio of

$\sqrt{2 \times 10^{-11}}$ or -53.5 dB for $t_2 = 1.0$ seconds referred to the pre-detection signal. Allowing about 5 times for the ratio of phase to amplitude modulation index, as before, we have for a saturating diode laser instead of a band limited thermal source, 67.5 dB referenced to incident optical power.

This compares with 72 dB that would come from shot noise, given an optical power of 100 microwatts into the detector; (69 db, given 10 microwatts into the detector).

It appears that it is the integrated bandwidth of the optical spectrum components that determines the low frequency fluctuations.

We conclude from this that intensity saturation in the source is very important and that the gain clamped broadband inhomogenous multimode laser is a better source for the Sagnac interferometer optical fiber gyro than either a more coherent source or a less coherent, non saturated (band limited thermal) source. A purely thermal but band limited source having no gain saturation smoothing at all could be disastrous. It may be objected that this is pessimistic, because a properly functioning super-radiant source would not have a mode structure. However, a mode structure consistent with the foregoing discussion is quite evident in high resolution spectrograms of the output from all super-radiant sources that we have observed.

C. The Effect of Scattering on Optical Fiber Gyros

1. Fluctuation and Error Due to Backscatter

Backscattering is imperfectly understood quantitatively. Inherent inhomogeneity in the fiber is known to be a primary source of (Rayleigh) scattering, and produces a well defined transmission loss in single mode fibers. A number of other factors, such as the capture angle of the scattered energy into the fiber, limit the scatter component trapped in the fiber, and mode stripping can be used to

minimize the level of the captured signal.

In the following we initially assume an idealized source whose 'incoherent' signal has the phase properties of simple band-limited noise but with constant intensity, and we assume that backscatter is principally due to Rayleigh scattering from sub-wavelength random inhomogeneities randomly distributed along the fiber. We neglect the effect of attenuation on the primary and scattered signal amplitudes and assume a uniform single polarization. We allow for temporal variation of the scattering in the fiber.

The signal returned from a cw Sagnac fiber interferometer at any instant may be expressed as the sum of the two primary waves that have traversed the loop in opposite directions but with very nearly the same delay, plus the coherent addition of two backscattered waves that have traveled the same distance (backscattered from the middle section of the fiber), plus uncorrelated wave components: backscattered from the rest of the fiber, plus quantum noise. To summarize:

$$E = E_r + E_l + E_{rsc} \exp(\phi_1) + E_{lsc} \exp(\phi_2) + E_{rsu} \exp(\phi_3) + E_{lsu} \exp(\phi_4) + \text{noise} \quad (III - 8)$$

E_r = (Vector) field strength of right hand wave

E_l = (Vector) field strength of left hand wave

E_{rsc} = Field strength of right hand scattered correlated wave

E_{lsc} = Field strength of left hand scattered correlated wave

E_{rsu} = Field strength of right hand scattered uncorrelated wave

E_{lsu} = Field strength of left hand scattered uncorrelated wave

(E^2 = Primary wave intensity referenced to the level reaching the detector, i.e., avoiding the attenuation factors.)

Waves scattered in the forward direction into the fiber are neglected since they travel with and are nearly synchronous in phase with their parent primary wave.

the phase (ϕ_n) of each of the backscattered waves relative to the primary signal waves is undetermined and not interrelated. The first two terms of the equation are constant in phase and intensity except as changes due to rotation, mechanical distortion, thermal expansion, intentional (bias) modulation, frequency drift or whatnot changes the effective nonreciprocal character of the fiber or modulates the signal by a "significant amount". A "significant amount" for our purpose, is on the order of the limit in sensitivity (on the order of 10^{-8} radians, or a length of 0.001 angstroms). The coherence time T of the "correlated" backscattering mechanism may be of finite duration, however, because of changes in the fiber, (i.e., changing birefringence, molecular motion, frequency drift, or some yet undetermined temporal effect). The correlation between the primary waves and the "correlated" backscatter waves may be less than the "integration time" (defined as T_2 of the receiving system, typically tens of seconds. All of the components are modulated, more or less, by the ac bias introduced at the ends of the loop at a frequency $v/(2L)$, where $v = c/n$ is the wave velocity and L is the length of the loop (Bergh 1981). The detector output is filtered at the same frequency.

In the following we use several symbols representing time elements:

- T is a time constant which accounts for the time variation of scattering in the fiber. This has been estimated to be 0.01 seconds (Ulrich 1980). Due to phase flicker or unstable mode structure in the laser source (Burns 1983) it could be much shorter.
- T_2 is the integration time of the receiver.
- τ is the coherence time (reciprocal bandwidth) of the incident signal, with spectrum density corresponding to a single mode spectrum.
- τ_1 is the coherence time corresponding to the bandwidth of a single line in

the multimode spectrum, (i.e., $= 1/B' = 1/\text{line width}$).

τ_2 is the coherence time corresponding to the spectrum envelope, (i.e., $= 1/\text{spectrum envelope width}$).

N is the number of modes in the spectrum.

t is a generalized time delay variable shorter than T , to be given a more specific value later.

t_2 is a time period. It may $= T_2$.

$\theta = nL/c$ is the single transit loop delay.

It frequently has been assumed that the "correlated" backscatter is constant, i.e., T is very large compared to t_2 . Even if it is constant, a frequency drift of the source or "spontaneous events" may reduce the correlation. A drift of one part in 10^5 or less may be sufficient to make T a significant factor.

The last terms in Eq. (III-8) vary in phase and amplitude with respect to the primary waves at a rate near $1/\tau$, where τ is the coherence time of the input signal. This is because the travel time from source to detector is different by more than the coherence time of the signal, so the components are from different signal epochs. This rate is very much higher than $1/T_2$. τ may be small or large, depending on the relative character of the source. For low coherence (semiconductor laser) sources, the overall signal bandwidth is measured in THz (Epworth 1982) as we have seen (Fig. III-3), with a duty factor between 0.1 and 0.01. τ is effectively of the order of 0.01 nanoseconds but some coherence effects may be spread over many nanoseconds. Coherence length is not a well defined quantity. In what follows we take τ_1 to be the reciprocal of the bandwidth of a single mode, and τ_2 to be that of the reciprocal of the bandwidth of the spectrum envelope. In Fig. III-3, $\tau_1 \simeq 10^{-10}$ and $\tau_2 = 10^{12}$.

When we use τ without a subscript, the integrated spectral density is presumed to apply. That is $N \cdot \tau_2$, where N is the effective number of laser modes.

Over a long period of time, all phases between the scatter products (Eq. III-8)) and the signal ($E_r + E_l$), (vector addition) are equally likely. On the average, the components will add in power, or with integration, in energy. We are interested in the threshold sensitivity (small nonreciprocity) so E_r and E_l are in phase. Taking the vector addition at the detector, $(E_r + E_l) = G$ is the signal reaching the detector. We start now with a primary signal of constant intensity (power) G^2 but randomly fluctuating in phase, with a coherence time τ . We combine with it (the result of backscatter in the fiber) another signal component of rms amplitude γ which has many parts which are delayed (multipath) by times much greater than τ . γ , then has a random, presumably Gaussian amplitude, random phase. Rayleigh intensity distribution. Combined with G , we expect an intensity with (rms) maxima momentarily in phase with G :

$$\text{Intensity} \quad I_1 = (G + \gamma)^2 \quad (\text{III} - 9)$$

Later we will account for the ac bias modulation and post detection filtering of the signal and scatter components.

If $\gamma \ll G$, the signal intensity maxima are adequately described by:

$$I_1 = (G^2 + 2G\gamma) \quad (\text{III} - 10)$$

with minima, similarly, $I_{\min} \simeq G^2 - 2G\gamma$. Averaged over intervals $t = \tau$ we expect to find fluctuations with a mean square value of:

$$q = \sqrt{2} G \gamma \tau \quad (\text{III} - 11)$$

on an average intensity $G^2\tau$, where $1/\sqrt{2}$ arises in going from maximum to mean square values. Over longer periods, t_2 , we expect an rms fluctuation:

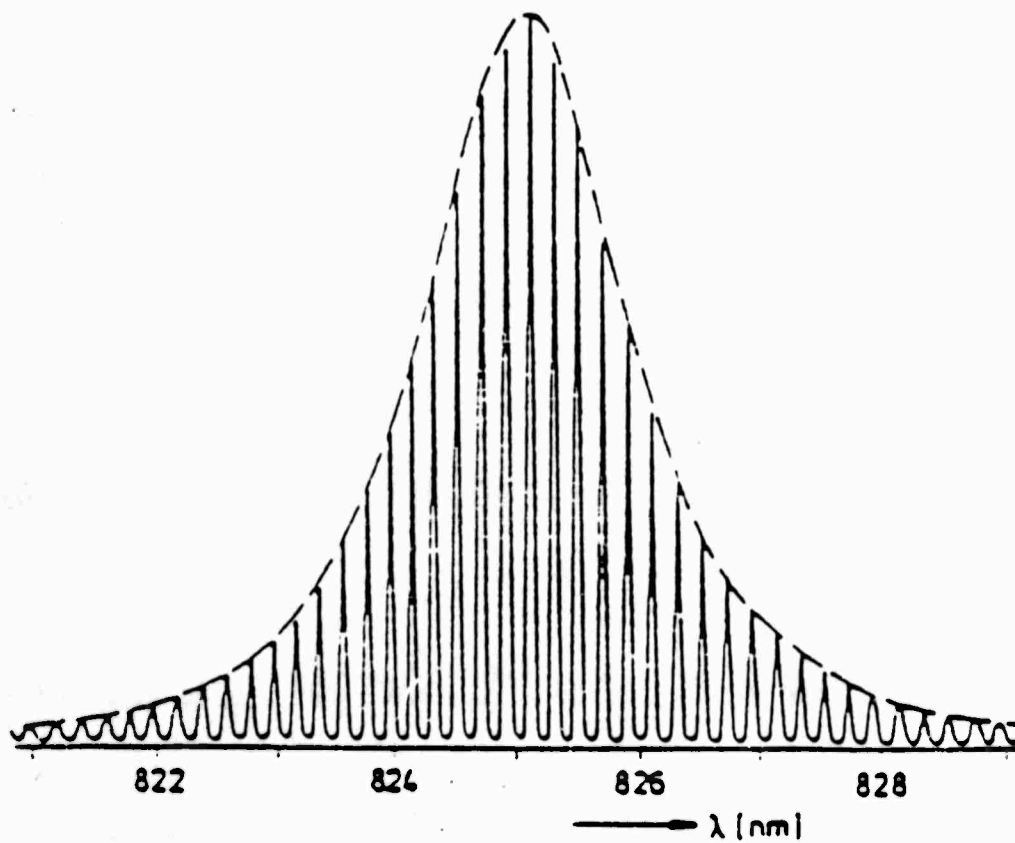


Fig. III-3. Typical spectrum of a multimode gain-guided laser (from Peterman 4/82). Because of gain saturation, amplitude fluctuations are about 1/5 what would be expected from the spectrum.

$$QI = \sqrt{2}G\gamma\tau \frac{\sqrt{t_2}}{\sqrt{\tau}} = \sqrt{2}G\gamma\sqrt{\tau t_2} \quad (III - 12)$$

where $t_2 \geq \tau$.

This fluctuation is on an average intensity: $G^2\tau t_2/\tau = G^2 t_2$.

Signal to noise is then:

$$\frac{1}{\sqrt{2}} \frac{G}{\gamma} \frac{\sqrt{t_2}}{\sqrt{\tau}} \quad (III - 13)$$

where G/γ is a dimensionless scattering coefficient.

There are different values of coherence for the waves scattered from different parts of the fiber so we will have to break this down in the next two sections.

Typically $\gamma^2 \simeq 2 \times 10^{-6} \cdot G^2$ watts per meter (see conclusion), so we get a ratio of scatter response to primary wave response, of the order -57 dB, for a rather coherent wave (coherence length = 1.0 meter). Clearly coherence is not always a good thing.

Now let us apply this relationship separately to the "correlated" and "uncorrelated" scatter components, and consider the effect of the baseband frequency offset due to modulation. This further complicates the analysis. We will use the above relations to apply more specifically to the Sagnac fiber gyro.

2. Correlated Components

Let us consider some consequences of the scatter components as influenced by the coherence times T , and τ_2 , and the integration time T_2 defined earlier. In the following we assume that the largest (i.e., only significant) loss mechanism in the fiber is Rayleigh scattering. The fraction of the scattered energy that is trapped in the fiber, the trapping factor, has been calculated for a representative case (Lin 1973, Stone 1970) to be 2.3×10^{-3} based on a trapping angle of 4.44 degrees and elimination of cladding modes. For an attenuation αl the ratio of the power in the

backscattered wave to the incident power for a small length ℓ is:

$$\alpha\ell = 2.3 \times 10^{-3}(1 - \exp^{-\alpha\ell}) \quad (III - 14)$$

or for α' in dB/meter and small attenuation

$$\sigma \approx 2.3 \times 10^{-3} \lambda \frac{\alpha\ell}{8.68} = 2.65 \times 10^{-4} \alpha'\ell \quad (III - 15)$$

Under stationary (no rotation) conditions the power in the combined correlated scatter components $E_{rsc} + E_{lsc}$ would be:

$$\text{Optical intensity} = 2E^2(\sigma N \tau_2 v) \quad (\text{power}) \quad (III - 16)$$

which replaces γ^2 in the previous section.

E^2 = the intensity of the clockwise or counter-clockwise waves, referenced to the detector position, and it is assumed to be equal in each direction.

σ = the backscatter constant, the ratio of backscatter to primary transmitted power, per unit length.

= (power scattered per meter/primary power)(trapping factor).

v = propagation velocity, no dispersion.

The two scattered components (right and left) are randomly phased, but add in power.

Over a period T , the correlated scatter signal adds coherently to the primary waves (E_r and E_l) giving a maximum integrated mean square error component, (from Eq. (III-11)):

$$\text{MS Error response, } Q = 2\xi GE \sqrt{\sigma N \tau_2 v} T \quad (\text{charge, or energy}) \quad (III - 17)$$

at some undetermined phase relative to the primary components. This we deduced as the maximum in-phase value and may be taken as accumulated charge in the post detection filter, or as optical energy accumulated over the time interval T . Though near constant during any interval T , it is random in phase, accumulating over longer times in a "random walk" process.

Ulrich (1980) has deduced a value of about 10^{-2} for T due to mechanical or thermal distortion of the fiber affecting the delay unsymmetrically or modifying the polarization of E a small amount introducing "phase noise". If, for instance, half of the fiber were lengthened by a half wavelength, the relative phase between the primary wave and scattered component would be changed by π radians. Variation of the source frequency would have the same effect. If we integrate in the receiver for a time T_2 , longer than T , successive samples of the "correlated" backscatter are uncorrelated (i.e., similar periods T have unrelated phases) so the total response for the longer period is (as in Eq. (III-12)):

$$\text{Integrated MS Error } Q_c = 2\xi GE \sqrt{\sigma N \tau_2 v} \sqrt{T T_2} \quad (\text{III} - 18)$$

where $T \leq T_2$.

This is the error voltage, (representing accumulated charge, or optical energy) which would be detected with a post detection filter at frequency = 0. However, generally the primary wave is phase modulated and the output is filtered at frequency $\nu/(2L)$ with a "lock-in" amplifier. We assume that the optical phase is modulated sinusoidally at an optimum level and that the detector is a balanced mixer followed by a simple low pass filter with a R-C time constant T_2 . Only the fluctuations at frequency $\nu/(2\theta)$ contribute to the charge accumulation Q_c . The output reflection from the exact center of the loop receives the oppositely phased modulation upon exiting the loop, emerges unmodulated and contributes nothing. But the scatter from points removed from the center by even a small increment

emerge with some modulation. On the average the correlated scatter is modulated by:

$$\text{Ratio of primary to scattered wave in-phase modulation} = \left[\frac{\pi\tau_1}{2\theta} \right]^2 \quad (\text{III} - 19)$$

times the modulation amplitude of the primary signal, as shown in the Appendix. The error (Eq. (III-18)) evidenced at the lock-in frequency must be reduced by this factor.

There is another possible contribution due to the "correlated" scatter, from the overlap of the wings (sidelobes) of the scatter bandwidth and the post detection bandwidth. As we have indicated, the 'correlated' backscatter is not really constant, but varies with a finite time constant T , presumably $\gg \tau_1$ and perhaps comparable to θ due to the environment or fiber variability. If the backscatter is modulated by any simple process, the amplitude of the modulation would be nearly constant within a bandwidth $1/T$ and finite outside, falling at some power of frequency. Let's assume the first power. In this case, the amplitude at the synchronous detection frequency $1/(2\theta)$ is either the same as at zero frequency (for T very small) or is reduced by a factor $2\theta/T$ (for $T \gg \theta$). Combining this with the residual phase modulation noted in the previous paragraph $(\pi\tau_1/(2\theta))^2$, Eq. (III-18) gives for the noise component in the synchronous detector band from the "correlated" scatter (power):

$$Q_c = 2\xi GE \sqrt{\sigma N \tau_2 v T T_2} \left[\left[\frac{2\theta}{T} \right]^2 + \left[\frac{\pi\tau_1}{2\theta} \right]^4 \right]^{1/2} \quad (\text{III} - 20)$$

Unless the source or the fiber is extremely unstable, or the source is very coherent, these factors are likely to be very small.

3. Uncorrelated Components

The peak power in the uncorrelated components, similarly, is:

$$\text{Uncorrelated Scatter} = 2E^2(\sigma(\theta - N\tau_2)v) \quad (\text{power}) \quad (III - 21)$$

where θ is the transit time of a signal in the fiber. This gives an rms current in the integrating square law detector (from Eq. III-11 as in Eq. III-17). (Equivalently, the effective power at the detector.)

$$I = 2\xi GE \sqrt{\sigma(\theta - N\tau_2)v} \quad (III - 22)$$

This signal component adds coherently only for a coherence time $N\tau_2$, and then incoherently. (Energy is cumulative up to T_2). Over the integration time T_2 , the integrated response is increased by $\sqrt{T_2}$, so:

$$Q_2 = 2\xi GE \sqrt{\sigma(\theta - N\tau_2)v} N\tau_2 \frac{\sqrt{T_2}}{\sqrt{N\tau_2}} \quad (III - 23)$$

The incoherent backscatter intensity is random and spread over a very wide band compared to the bias modulation frequency. The bias modulation shifts this band too, but the band is very broad so the intensity falling into the post detection filter is unchanged. We are interested in the relative fluctuation, so we compare this with the average signal intensity (or output from the detector). The average signal intensity is given by the first term in Eq. (III-10), times the integration time T_2 , i.e., $Q_0 = \xi G^2 T_2$. Altogether, then, we have a fluctuation to dc output ratio:

$$\frac{Q_2}{Q_0} = 2 \frac{E}{G} \sqrt{\sigma N\tau_2 v} \frac{\sqrt{T}}{\sqrt{T_2}} \left[\left[\frac{2\theta}{T} \right]^2 + \left[\frac{\pi\tau_1}{2\theta} \right]^4 + \frac{\theta - N\tau_2}{T} \right]^{1/2} \quad (III - 24)$$

where $T \leq T_2$.

The first two terms in the bracket serve to warn against using sources of high temporal coherence and to account for variability in the fiber or the source.

The value of E/G is deduced in the Appendix for optimum phase modulation and synchronous detection as having a value of 1.5.

4. Scatter Equivalent Phase and Rotation Error

In the Appendix we obtain a relationship for the noise equivalent phase error:

$$\phi' = \frac{1}{1.27} \frac{V(rms)}{V(dc)} = \frac{1}{1.27} \frac{Q_s}{Q_0} \quad (III - 25)$$

This is, from Eq. 24, when $\theta \ll T$ and $\tau_1 \ll \theta$:

$$\phi' = 3.34 \sqrt{\sigma N \tau_2 v \theta / T_2} \quad (III - 26)$$

of more interest, perhaps, is the noise equivalent rotation rate. Since the perceived rotation rate is:

$$\Omega' = \frac{c\lambda}{4\pi RL} \phi' \quad (III - 27)$$

(reference Bergh 1981) we have an (rms) noise equivalent rotation rate (substituting $L = \theta v$):

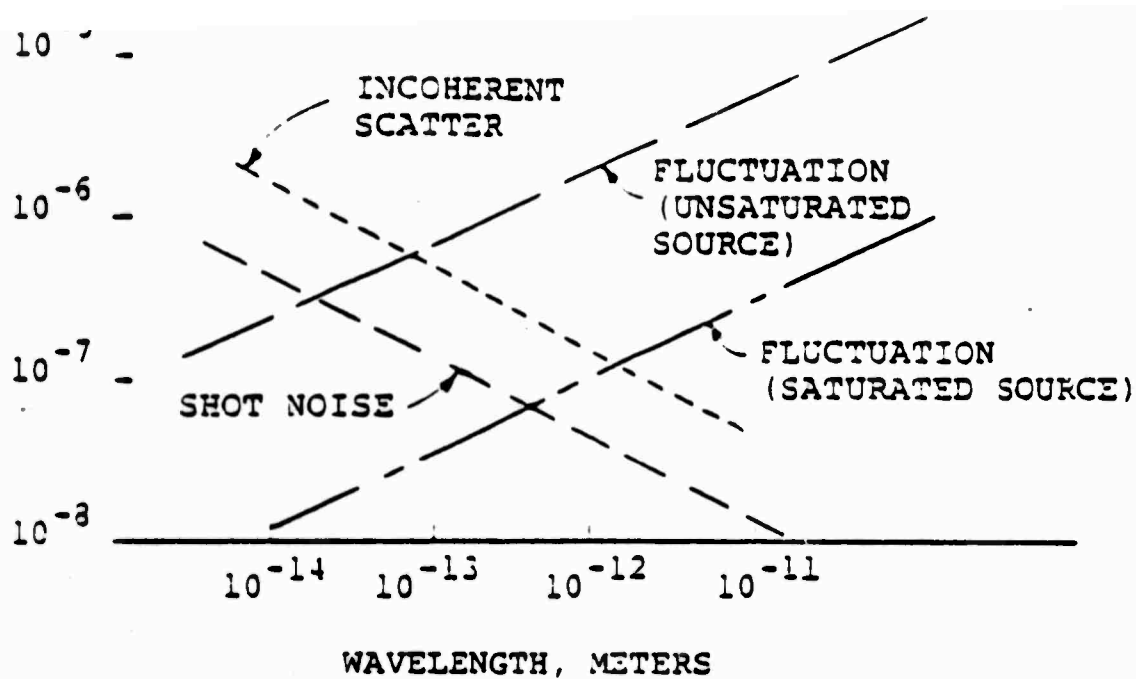
$$\Omega' = 0.84 \frac{c\lambda}{\pi R} \frac{\sqrt{\sigma N \tau_2}}{\sqrt{L T_2}} \quad (III - 28)$$

where we have neglected the "correlated" scatter components.

Using the foregoing equations, and the "representative values" given below we get a noise equivalent phase error of 1.5×10^{-7} radians (rms) or a noise equivalent rotation rate of

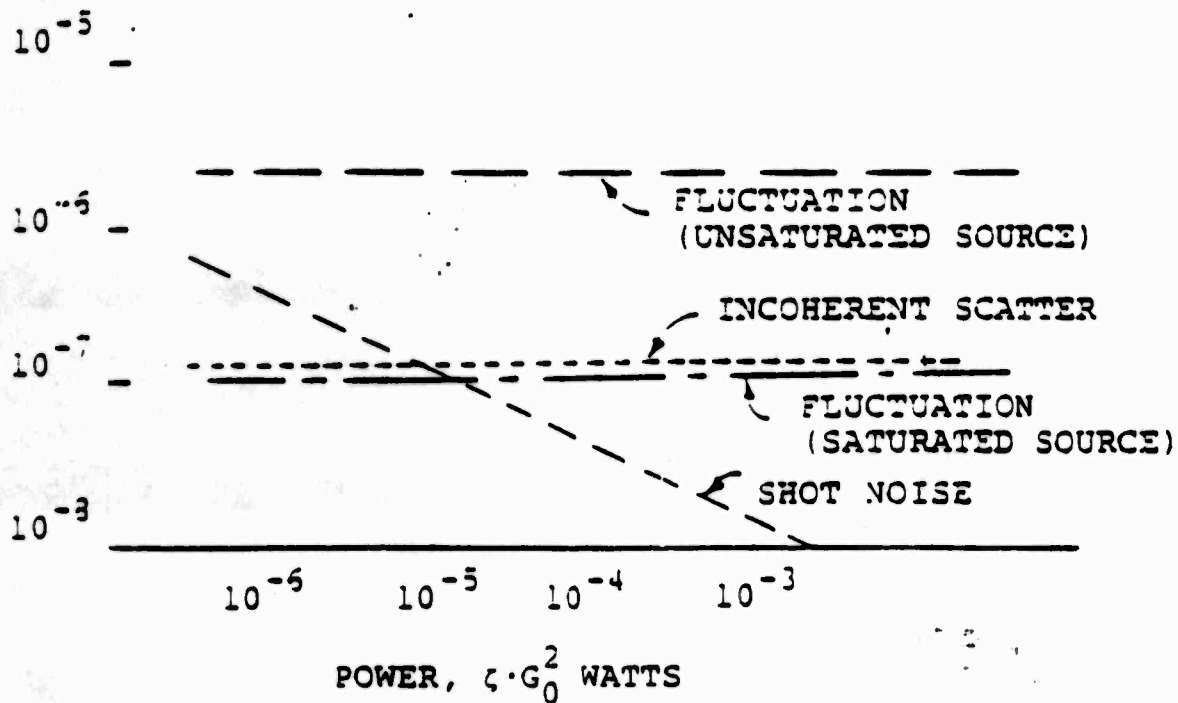
$$\Omega' = 1.28 \times 10^{-7} \text{ rad/sec} \quad (III - 29)$$

This compares to a value (shot noise equivalent phase error) of 4.8×10^{-8} for shot noise, and 1.2×10^{-7} for the fluctuation of the assumed multimode gain saturating semiconductor laser having the same bandwidth. These relations can be seen in Fig. III-4.



(a)

NOISE EQUIVALENT ROTATION RATE



(b)

Fig. III-4. Comparison of the three principal sources of noise (i.e., primary signal fluctuations, uncorrelated scatter, and shot noise); (a) as a function of wavelength at a power of 10^{-4} watts, and (b) as a function of power at a wavelength of one micrometer.

$\alpha' = 1 \text{ dB/km}$	$\lambda = 1 \text{ micrometer}$
$T = 0.01$	$T_2 = 1.0$
$\sigma = 5 \times 10^{-7} \text{ m}$	$\theta = 2 \times 10^{-6}$
$R = 0.07 \text{ m}$	$L = 400 \text{ m}$
$\tau = 10^{-11}$	$\tau_1 = 10^{-10}$
$\tau_2 = 10^{-12}$	$N = 10$
$v = 2 \times 10^8$	$G^2 = 10^{-4} \text{ watts}$
$f = 3 \times 10^{14}$	$\xi = 1.0$
$n = 1.5$	

If we increase the wavelength by a factor k , scaling the fiber diameter and nothing else, the Rayleigh scatter is reduced by k^4 . So one might suppose that there was a big advantage in going to longer wavelengths. However, the 'noise equivalent rotation rate' is reduced only by k^1 and the sensitivity to rotation is reduced by the same factor. Thus, if the gyro is limited by scatter there appears to be a standoff. Other factors, such as source coherence length are likely to be important.

A. Sensitivity of Sagnac Effect, using an AC bias

The receiving system in a fiber gyro is designed to measure the departure from reciprocity of the counter propagating waves caused by rotation in the plane of the fiber loop. The non-reciprocal port of the interferometer gives a signal level (volts) proportional to the cosine of the anti-reciprocal component, and if there is no bias, is least sensitive at low rotation rates. Phase modulation, by piezo-electrically stretching the fiber sinusoidally, and synchronous detection, is used to maximise the sensitivity. With primary waves E_r and E_l equal, and modulating the phase at a rate π/θ , we get, at the reciprocal port:

$$E = |E_r| \cos(\omega t + \phi + \phi') + |E_l| \cos(\omega t - \phi - \phi') \quad (1)$$

where $E_2 =$ wave intensity, and

$$\phi = \phi_0 \cos(\pi t/\theta) \quad (2)$$

represents the non-reciprocal modulation bias applied at the end(s) of the loop, and ϕ' represents the phase components due to rotation and other non-reciprocal factors.

For our present purposes, $\phi' \ll \phi$ and $|E_r| = |E_l| = E_0$, and we define $b = \pi t/\theta$. Thus:

$$E = E_0(\cos(\omega t + \phi + \phi') + \cos(\omega t - \phi - \phi')) \quad (3)$$

From a trigonometrical identity, we have:

$$E = 2E_0 \cos(\phi + \phi') \cos(\omega t) \quad (4)$$

This is an optical sinusoidal carrier with an envelope:

$$\text{Envelope} = \cos(\phi + \phi') = \cos(\phi_0 \cos(b) + \phi') \quad (5)$$

$$= \cos(\phi) \cos(\phi') - \sin(\phi) \sin(\phi') \quad (6)$$

for small ϕ' , $\cos(\phi') \simeq 1$, and $\sin(\phi') \simeq \phi'$, and:

$$\text{Envelope} \simeq \cos(\phi) - \phi' \sin(\phi) \quad (7)$$

The intensity is:

$$V = \cos^2(\phi) - 2\phi' \sin(\phi) \cos(\phi) + \phi'^2 \sin^2(\phi) \quad (8)$$

The first term contains dc and terms of even order in π/θ . The last term is very small for small ϕ' . The second term is the only one which is linear in ϕ' and contains components at the fundamental modulation frequency $1/2\theta$. Thus,

$$V_2 = -2\phi' \sin(\phi) \cos(\phi) = -\phi'(\sin(\phi - \phi) - \sin(2\phi)) \quad (9)$$

$$= 0 - \phi' \sin(2\phi) \quad (10)$$

See footnote.

Expressing the sine function in a series, we get:

$$V_2 = -\phi'(2\phi - \frac{2^3 \phi^3}{3!} + \frac{2^5 \phi^5}{5!} - \dots) \quad (11)$$

* FNH Robinson points out that this is a Bessel equation, and that the fundamental spectral component could be obtained conveniently using a Fourier transform. See: Handbook of Math Functions, Abramowitz and Stegun, NBS 1964, p. 360. Also "A Treatise on the Theory of Bessel Functions," Watson, Cambridge, 1958, section 9.4.

$$= -\phi' \left[2\phi_0 \cos(b) - \frac{2^3}{3!} \phi_0^3 \cos^3(b) + \frac{2^5}{5!} \phi_0^5 \cos^5(b) + \dots \right] \quad (12)$$

We want to extract the part containing frequency $1/2\theta$, (i.e., the cosine argument $= b$, with no multiplier).

we use

$$\cos^3(b) = \frac{3}{4} \cos(b) + \frac{1}{4} \cos(3b) \quad (13)$$

and

$$\cos^5(b) = \frac{5}{8} \cos(b) + \frac{5}{16} \cos(3b) + \dots \quad (14)$$

which gives

$$V_2 = -\phi' \cos(b) \left(2\phi_0 - \phi_0^3 + \frac{1}{8} \phi_0^5 - \dots \right) \quad (15)$$

This is maximum (absolute) when $\phi_0 = .94$ radians, or 53 degrees. That is, 106 degrees phase difference between counter propagating waves.

Substituting for b and ϕ_0 in Eqs. (8) and (15), we have from the square law detector:

$$V = \cos^2(\phi) - 1.17 \cos(\pi t/\theta) \phi' \quad (16)$$

We need to compare this with the dc component from the detector. That is contained in the $\cos^2(\phi)$ term.

$$\cos^2(\phi) = \frac{1}{2} (1 + \cos(2\phi)) \quad (17)$$

$$= \frac{1}{2} [1 + \cos(2\phi_0 \cos(b))] \quad (18)$$

$$= \frac{1}{2} \left[1 + 1 - \frac{2^2 \phi_0^2 \cos^2(b)}{2!} + \frac{2^4 \phi_0^4 \cos^4(b)}{4!} - \dots \right] \quad (19)$$

$$= \frac{1}{2} \left[2 - \frac{2^2}{2!} \phi_0^2 \frac{1}{2} + \frac{2^4}{4!} \phi_0^4 \frac{1}{4} (1 + \cos(2b))^2 \frac{2^6}{6!} \phi_0^6 \frac{1}{8} (1 + \dots)^3 \right] \quad (20)$$

(We have dropped harmonic frequencies like $\cos(2b)$.)

$$= 1 - \frac{1}{2!} \phi_0^2 \frac{1}{2} + \frac{2^3}{4!} \cdot \frac{1}{4} \cdot \frac{3}{2} \cdot \phi_0^4 - \frac{2^5}{6!} = \frac{1}{8} \cdot \frac{5}{2} \phi_0^6 \dots \quad (21)$$

$$= 1 - \phi_0^2/2 + 3/4! \phi_0^4 - 10/6! \phi_0^6 \dots \quad (22)$$

$$= 0.65 \quad (\text{for } \phi_0 = 0.94)$$

This corresponds to the average intensity seen by the detector, or the value of G/E required for Eq. (III-24).

So we have the ratio of the maximum lock-in output to the dc:

$$\frac{V_2(max)}{V(dc)} = \frac{1.17\phi'}{0.65} = 1.8\phi' \quad (23)$$

or

$$\frac{V(rms, max)}{V(dc)} = 1.27\phi' \quad (24)$$

In the absence of rotation, ϕ' is the "noise equivalent phase error" used in Eq. (III-26).

B. AC Bias Modulation of the "Correlated" Scatter

The bias phase modulation is assumed to be applied in equal amounts out of phase, at each end of the fiber loop, (conceptually, since it makes no difference if it is all at one end). The modulation of the primary wave is $\phi' = (1/2)\phi_0 \cos(\pi t/\theta)$, and the modulation is doubled at the other end of the loop because the chosen phase of the modulation in the two modulators. Waves scattered back from the exact center of the loop are modulated again, but with the opposite phase, and thus emerge with no modulation. Waves scattered from points slightly removed from the center of the loop by a distance d emerge with total phase modulation:

$$\phi_s = \frac{1}{2}\phi_0 \left[\cos\left(\frac{\pi}{\theta}t\right) + \cos\left(\frac{\pi}{\theta}t + \frac{\pi(\theta - 2dv)}{\theta}\right) \right] \quad (25)$$

For a signal with coherence time τ_1 the mean value of $|2dv| = \tau_1$ giving a phase modulation, for $(\tau_1 \ll \theta)$,

$$\phi_s = \frac{1}{2}\phi_0 \left[\cos\left[\frac{\pi}{\theta}t\right] + \cos\left[\frac{\pi}{\theta}t + \pi + \frac{\pi\tau_1}{\theta}\right] \right] \quad (26)$$

$$= \frac{1}{2}\phi_0 \left[\cos\left(\frac{\pi}{\theta}t\right) - \cos\left(\frac{\pi}{\theta}t\right)\cos\left(\frac{\pi\tau_1}{\theta}\right) - \sin\left(\frac{\pi}{\theta}t\right)\sin\left(\frac{\pi\tau_1}{\theta}\right) \right] \quad (27)$$

The sine term is in quadrature with the synchronous detector and is tuned out.

We have left, substituting:

$$1 - \frac{1}{2}\left[\frac{\pi\tau_1}{\theta}\right]^2 \quad \text{for} \quad \cos\left[\frac{\pi\tau_1}{\theta}\right] \quad (28)$$

$$\phi_s \simeq \frac{1}{2}\phi_0 \frac{1}{2}\left[\frac{\pi\tau_1}{\theta}\right]^2 \cos\left[\frac{\pi}{\theta}t\right] \quad (29)$$

So, the ratio of the coherent scattering to primary wave phase modulation is:

$$\frac{\phi_s}{\phi_0} = \left[\frac{\pi\tau_1}{2\theta}\right]^2 \quad (30)$$

C. Shot Noise Output

The shot noise from the detector is:

$$i_s^2 = 2ei_0B \quad (31)$$

on a current i_0 , and,

$$i_0 = \xi \frac{G_0^2}{hf} e \quad (32)$$

where G^2 , still, is intensity. i.e., watts.

Substituting:

$$\frac{I_s^2}{i_0^2} = \frac{2Bhf}{\xi G_0^2} \quad (33)$$

Comparing this with Eq. (24), we get the shot noise limit on ϕ' :

$$\phi'(rms) = \frac{1}{1.27} \frac{\sqrt{2Bhf}}{\sqrt{\xi G_0^2}} \quad (34)$$

or a 1.0 Hz bandwidth and $\xi = 1.0$ and $G_0^2 = 10^{-4}$ watts, Plancks constant $h = 6.26 \times 10^{-34}$, and $f = 3 \times 10^{14}$ Hz, we get $I_s^2/I_0^2 = 4 \times 10^{-15}$ and $\phi' = 5 \times 10^{-8}$ radians. Referenced to the optical signal, the fluctuation to average power ratio is 6.3×10^{-8} , i.e., 4.5 dB lower than the fluctuation noise calculated for the gain saturated multimode laser in the text of this paper, and 13 dB lower than the fluctuation from the assumed broad band unsaturated superradiant source, (see Eqs. (III-4) and (III-6).

v. BIBLIOGRAPHY

1. K. Peterman, "Intensity-dependent Nonreciprocal Phase Shift in a Fiber-optic Gyroscope for Light Sources with Low Coherence," *Opt. Lett.* **7**, 623-625 (1982).
2. K. Vahala and A. Yariv, "Semiclassical Theory of Noise in Semiconductor Lasers: Parts I and II," *IEEE J. of Quant. Electr.* **QE-19**, 1096-1109 (1983).
3. C. H. Henry, "Theory of the Line Width of Semiconductor Lasers," *IEEE J. of Quant. Electr.* **QE-18**, 259-264 (1982).
4. S. D. Personick, *Optical Fiber Transmission Systems*, Plenum Press, 124-125 (1981).
5. S-C. Lin, and T. G. Giallorenzi, "Sensitivity Analysis of the Sagnac-effect Optical Fiber Ring Interferometer," *Appl. Opt.* **18**, 915 (1979).
6. J. Stone, "Measurement of Rayleigh Scattering in Liquids using Optical Fibers," *Appl. Opt.* **12**, 1824 (1973).
7. M. Tur, and B. Moslehi, "Laser Phase Noise Effects in Fiber-optic Signal Processors with Recirculating Loops," *Opt. Lett.* **8**, 229-231 (1983).
8. W. R. Bennett, "Noise Characteristics and Origins," *Electronics* **29**, 154 (1956).
9. H. R. Rowe, "Amplitude Modulation with a Noise Carrier," *Proc. IEEE* **52**, (1964).
10. H. R. Rowe, "Theory of Two-photon Measurement of Laser Output," *IEEE J. Quant. Electr.* **QE-6**, 49-67 (1970).
11. S. O. Rice, "Mathematical Analysis of Random Noise," *BSTJ* **23** 282-332 (1944); *BSTJ* **24**, 46-156 (1945).
12. W. C. Jakes, *Microwave Mobile Communications*, Wiley, 59 and 189 (1974).
13. J. W. Goodman, *Statistical Optics*, Wiley (1983).
14. J. R. Pierce and E. C. Posner, *Introduction to Communication Science and Systems*. Plenum Press (1979).
15. R. A. Bergh, R. C. Lefevre, and H. J. Shaw, "Compensation of the Optical Kerr Effect in Optical Fiber Gyroscopes," *Opt. Lett.* **7**, 282-284 (1982).
16. A. Dandridge and A. B. Tveten, "Properties of Diode Lasers with Intensity Noise Control," *Appl. Opt.* **22**, (1983).
17. A. Yariv and W. Caton, "Frequency, Intensity, and Field Fluctuations in Laser Oscillators," *IEEE J. Quantum Electron.* **QE-10**, 509-515 (1974).
18. N. J. Frigo, H. F. Taylor, L. Goldberg, J. F. Weller, and S. C. Rayleigh,

"Optical Kerr Effect in Fiber Gyroscopes: Effects of Nonmonochromatic Sources," *Opt. Lett.* **8**, 119-121 (1983).

19. R. E. Epworth, "The Temporal Coherence of Various Semiconductor Light Sources used in Optical Fiber Sensors," *Springer Series in Optical Sciences* **32**, 237-249 (1982).
20. R. A. Bergh, B. Culshaw, C. C. Cutler, H. C. Lefevre, and H. J. Shaw, "Source Statistics and the Kerr Effect in Fiber-optic Gyroscopes," *Opt. Lett.* **7**, 563-65 (1982).
21. C. C. Cutler, S. A. Newton, and H. J. Shaw, "Limitation of Rotation Sensing by Scattering," *Opt. Lett.* **5**, 488-490 (1980).
22. R. Ulrich, "Fiber Optic Rotation Sensing with Low Drift," *Opt. Lett.* **5**, 173-175 (1980).
23. R. A. Bergh, H. C. Lefevre and H. J. Shaw, "All Single Mode Fiber Optic Gyroscope with Long-term Stability," *Opt. Lett.* **6**, 502-504 (1981).
24. H. E. Rowe, *Signals and Noise in Communication Systems*, Princeton N. J. Van Nostrand, 118 (1965).
25. A. Dandridge and H. F. Taylor, "Correlation of Low Frequency Intensity and Frequency Fluctuations in GaAlAs Lasers," *IEEE J. Quant. Electr.* **QE-18**, 1738-1750 (1982).
26. A. Dandridge and A. B. Tveten, "Phase Noise of Single-mode Diode Lasers in Interferometer Systems," *Appl. Phys. Lett.* **39**, 530-532 (1981).
27. K. Peterman, and G. Arnold, "Noise and Distortion Characteristics of Semiconductor Lasers in Optical Fiber Communication Systems," *IEEE J. Quant. Electr.* **QE-18**, 543-555 (1982).
28. K. Peterman and E. Weidel, "Semiconductor Laser Noise in an Interferometer System," *IEEE J. Quant. Electr.* **18**, 1251-1256 (1981).
29. C. Harder, K. Vahala, A. Yariv, "Measurement of the Line Width Enhancement Factor α of Semiconductor Lasers," *Appl. Phys. Lett.* **42**, 328-330 (1983).
30. T. K. Yee, "Study of Intensity Noise of GaAlAs Laser Diodes at Various Output Powers and Frequencies," *CLEO*, Baltimore, 1983.
31. K. Bohm, P. Marten, K. Peterman, E. Weidel, and R. Ulrich, "Low-drift Fibre Gyro using a Superluminescent Diode," *Electr. Lett.* **7**, 352-53 (1981).
32. K. Bohm, P. Russer, K. Weidel and R. Ulrich, "Low Noise Fiber Optic Rotation Sensing," *Opt. Lett.* **6**, 64-66 (1981).
33. W. K. Burns and R. P. Moeller, "Rayleigh Backscattering in a Fiber Gyroscope with Limited Coherence Sources," *IEEE Journal of Lightwave Technology*, **LT-1**, 2, 381-386 (1983).